UCRL-11143

University of California
Ernest O. Lawrence Radiation Laboratory

TWO-WEEK LOAN COPY

This is a Library Circulating Copy which may be borrowed for two weeks. For a personal retention copy, call Tech. Info. Division, Ext. 5545

POLARIZATION OF SILVER NUCLEI IN FERROMAGNETS AND THE INTERNAL MAGNETIC FIELD

Berkeley, California

DISCLAIMER

This document was prepared as an account of work sponsored by the United States Government. While this document is believed to contain correct information, neither the United States Government nor any agency thereof, nor the Regents of the University of California, nor any of their employees, makes any warranty, express or implied, or assumes any legal responsibility for the accuracy, completeness, or usefulness of any information, apparatus, product, or process disclosed, or represents that its use would not infringe privately owned rights. Reference herein to any specific commercial product, process, or service by its trade name, trademark, manufacturer, or otherwise, does not necessarily constitute or imply its endorsement, recommendation, or favoring by the United States Government or any agency thereof, or the Regents of the University of California. The views and opinions of authors expressed herein do not necessarily state or reflect those of the United States Government or any agency thereof or the Regents of the University of California.

UCRL-11143
UC-4 Chemistry
TID 4500(24th Ed.)

Research and Development

UNIVERSITY OF CALIFORNIA

Lawrence Radiation Laboratory
Berkeley, California

AEC Contract No. W-7405-eng-48

POLARIZATION OF SILVER NUCLEI IN FERROMAGNETS AND THE INTERNAL MAGNETIC FIELD

Gene A. Westenbarger

(Thesis)

November 21, 1963

Printed in USA. Price $2.25. Available from the
Office of Technical Services
U. S. Department of Commerce
Washington 25, D.C.

POLARIZATION OF SILVER NUCLEI IN FERROMAGNETS AND THE INTERNAL MAGNETIC FIELD

Contents

Abstract v

I. Introduction 1

II. Theory of Nuclear Polarization

- A. General Discussion 3
- B. Orientation Parameters 4
- C. Gamma Radiation 6
- D. Allowed Beta Decay 7

III. Experimental Equipment

- A. Demagnetization Cryostat 10
- B. Electromagnet 13
- C. Magnetic Thermometer 14
- D. Radiation Detectors 14
- E. Polarizing Magnet 16
- F. Alloy Preparation 20
- G. Thermal-Contact Assembly 21

IV. Experimental Procedure 28

V. Thermometry

- A. Magnetic Thermometer 31
- B. Co^{60} Thermometer 35

VI. Results

- A. Decay Scheme of Ag^{110m} 41
- B. Magnitude of the Hyperfine Interaction 53
- C. Sign of the Hyperfine Interaction 60
- D. Polarization of Ag^{104} 74

VII. Discussion

- A. Other Methods 83
- B. Comparison with Other Work 84
- C. Origin of the Internal Field 87

D. Conclusions 92
Acknowledgments 93
References 94

POLARIZATION OF SILVER NUCLEI IN FERROMAGNETS AND THE INTERNAL MAGNETIC FIELD

Gene A. Westenbarger

Department of Chemistry and Lawrence Radiation Laboratory
University of California, Berkeley, California

November 21, 1963

ABSTRACT

The signs and magnitudes of the hyperfine-structure constants of two silver isotopes dissolved in the ferromagnetic metals iron and nickel have been determined. The silver nuclei were polarized by application of a small magnetic field to alloys that had been cooled to near 0.01°K. Thermometry was performed by measurement of the polarization of Co^{60} in the alloy. Spatial anisotropies of both beta and gamma rays from Ag^{104} and Ag^{110m} were measured. Parity was shown not to be conserved in the allowed beta decay of these isotopes. Spin assignments were made or confirmed for several excited states in Cd^{110}. The M1-E2 mixing ratios were determined for the 1384-keV and 1504-keV γ rays following the decay of polarized Ag^{110m}. The products of the nuclear magnetic moment of Ag^{110m} and the internal magnetic fields at the nuclei of silver dissolved in iron and nickel were found to be negative and equal to $-(9.0 \pm 0.5) \times 10^5$ nm gauss for Ag^{110m} in iron and $-(3.5 \pm 0.3) \times 10^5$ nm gauss in nickel. The role of conduction-electron polarization in the production of internal magnetic fields in ferromagnetic metals is discussed.

I. INTRODUCTION

The pioneering experiments of Samoilov in 1959 showed that, under certain conditions, the nuclei of diamagnetic elements may be polarized when dissolved in a ferromagnetic metal.[1,2] This new method of nuclear polarization has been used primarily for determination of the magnetic fields at the nuclei of several diamagnetic impurity elements dissolved in iron. These hyperfine magnetic fields are generally found to be large and may be of the order of several hundred kilogauss.[3] For every case, except one,[4] in which the sign of the internal field has been determined, the sign has been found to be directed oppositely to the bulk magnetization of the metal.[5,6,7]

The internal fields in metals are of major importance to the theory of the solid state. The origin of these large negative internal fields lies in the electronic structure of the metal and has been a subject of much recent discussion.[8,9] At present, insufficient knowledge exists to formulate a complete theory that would allow calculation of the various contributions to the internal magnetic field. There is strong indication, however, that polarization of the nuclei of diamagnetic elements is produced through polarization of the outer s electrons of the diamagnetic atoms by the conduction s electrons of the metal. Thus, study of the s-electron contribution to the observed fields is desirable.

The elements Cu, Ag, and Au form the IB subgroup of the periodic system of the elements and have the valence configurations $4s^1$, $5s^1$, and $6s^1$, respectively. Recently, the internal fields at the nuclei of Cu in iron and cobalt[10] and in nickel[11] and at Au nuclei in iron, cobalt, and nickel have been measured.[6,12] The signs of the fields have been determined in the Au alloys and for Cu in nickel. One objective of this research was to extend this series of measurements by a study of the sign and magnitude of the hyperfine structure of Ag in iron and in nickel alloys.

Ferromagnetic nuclear polarization can also be a powerful tool for nuclear physics. It allows the study of the nuclear properties of many isotopes heretofore not possible and is excelled in this respect only by the "brute force" method of nuclear polarization, which has been realized experimentally in only one favorable case.[13] Major contributions to the theory of beta decay and other nuclear phenomena may result from this now secondary use of nuclear polarization in ferromagnetic metals. In this work a step is taken toward realization of this potential.

Presented first is a summary of the theory of nuclear polarization; this is followed by a description of the new experimental technique. The results of polarization of Ag^{110m} and Ag^{104} are then given and analyzed in detail. Both the nuclear properties and the metallic hyperfine interactions are discussed. A qualitative description of the origin of the internal fields for diamagnetic elements is given in a final section.

II. THEORY OF NUCLEAR POLARIZATION

A. General Discussion

The general theory of low temperature nuclear orientation has been formulated by several authors.[14, 15, 16] Only the specific part of this theoretical treatment that is applicable to the polarization of nuclei in ferromagnetic metals is summarized here.

Polarization of nuclei in a ferromagnet arises through the interaction of the nuclear magnetic dipole moment with a magnetic field that is fixed in space. The 2I+1 magnetic hyperfine sublevels are degenerate in the absence of a magnetic field, but in a field this degeneracy is completely removed. The energy of a particular level then depends upon the magnetic quantum number I_z. The energy splitting is determined by the energy of the nuclear dipole in the field and is given by

$$\mathcal{H} = -\mu \cdot H = g_N \beta_N H_z I_z \,, \tag{1}$$

where $\mathcal{H}$ is the nuclear part of the Hamiltonian, μ is the nuclear magnetic moment, and H is the magnetic field at the nucleus. The second expression gives the energy in the usual spin-Hamiltonian notation. Here g_N is the nuclear g factor, β_N is the nuclear magneton, H_z is the hyperfine magnetic field, and I_z is the z component of the nuclear spin, which is just the usual magnetic quantum number m. The levels are separated equally in energy and the energy difference between levels is $\mu H/I$.

In thermal equilibrium the nuclei are distributed among these magnetic levels, the populations of which are governed by a Boltzmann function,

$$W(m) = \frac{\exp(-E_m/kT)}{\sum_m \exp(-E_m/kT)} \,,$$

where $W(m)$ is the fractional population of the level m, E_m is the

energy of this level, k is the Boltzmann constant, and T is the absolute temperature of the system.

In spite of the large magnetic fields that exist at the nuclear position in ferromagnetic metals, the interaction energy is extremely small, being typically of the order of 3×10^{-6} eV. This corresponds to a thermodynamic temperature (kT) of the order of 0.03°K. Thus, at temperatures above this order of magnitude, the populations of the levels are essentially equal and no polarization of the nuclei occurs. The material must, therefore, be cooled to a very low temperature before appreciable polarization can exist. That is, if,

$$\beta \equiv \frac{\mu H}{I k T} \approx 1 , \tag{2}$$

the degree of polarization increases as β is made large.

The magnetic field that produces the polarization must be fixed in space. Since it is produced by the electrons in the metal, the direction of the field in space is determined by the direction of the atomic moments in the material. In a ferromagnet these moments lie parallel within a Weiss domain. A polycrystalline material contains domains of all orientations with a net magnetization resulting only from hysteresis effects. The domains may be made to lie parallel by applying sufficient external field to saturate the magnetization of the material. In this state all domains lie parallel and are polarized. The field at the nucleus then lies along the external field, but may be directed oppositely to the atomic moments.

B. Orientation Parameters

The angular distribution of radiation from polarized nuclei may be represented by the function

$$W(\theta) = \sum_{k=0}^{\lambda} B_k U_k F_k P_k . \tag{3}$$

The functions B_k, U_k, and F_k each depend upon a variety of atomic and nuclear parameters and will be formulated more fully below. The

function P_k is the Legendre polynomial of order k having argument $\cos\theta$, where θ is the angle between the axis of magnetization and the direction of emission of the radiation. The expansion is valid for λ equal to $2I$ or $2L$, whichever is smaller. For $k > 2I$, $B_k = 0$ and for $k > 2L$, $F_k = 0$, where L is the angular momentum carried away from the nucleus during decay and I is the angular momentum of the nucleus before decay. Successive terms of the expansion in Eq. (3) decrease rapidly. At currently attainable temperatures only terms through $k = 4$ have been required to fit the experimental radiation distribution.

The functions B_k describe the degree of nuclear orientation. Oriented nuclei are said to be "aligned" if the orientation depends upon only the even terms of the expansion, and to be "polarized" if the odd terms, especially the $k = 1$ term, appear. In alignment, the hyperfine substates remain partially degenerate; that is, the $+m$ and $-m$ levels have the same energy. If this degeneracy is removed by application of an external field, one direction along the axis is enhanced with respect to the opposing direction and polarization occurs. The complete removal of the magnetic degeneracy in a ferromagnetic metal by the internal field gives rise to nuclear polarization rather than nuclear alignment in these materials.

The following expressions were used for the calculation of B_0, B_1, and B_2 in this work:

$$B_0 \equiv 1,$$

$$B_1 = \frac{2}{\sqrt{3}} \sum_m m\, W(m) ,$$

$$B_2 = \sum_m \frac{[m^2 - I(I+1)/3]}{(1/5)[I(I+1)(2I-1)(2I+3)]} W(m) . \tag{4}$$

The general expression for B_k is

$$B_k = \sqrt{2k+1} \sum_m C^{IkI}_{m0m} W(m) ; \tag{5}$$

Equation (5) was used for calculation of B_4, where C is the Clebsch-Gordan coefficient having the indices shown.

C. Gamma Radiation

The functions U_k in Eq. (3) account for the reorientation occurring during transitions that precede the emission of the detected quantum. These functions are dependent upon the angular momenta of all the levels through which the decay has proceeded as well as on the multipole character of each of these transitions. Explicit forms for the U_k for transition of both pure and mixed multipole character are given in reference 14.

The F_k functions depend upon the multipole character of the observed transition and upon the angular momenta of the initial and final nuclear states. These are the same geometric functions that appear in the theory of angular correlation. The F_k functions are also defined in reference 14. For an unmixed transition, F_k is given by

$$F_k = (-)^{I_f - I_i - 1} (2I_i + 1)\, C \begin{matrix} L & L & k \\ 1 & -1 & 0 \end{matrix}\; W(I_i I_i LL;\, k I_f) ,$$

where I_i and I_f are respectively the initial and final nuclear spins and W is a Racah coefficient.

For γ radiation the functions F_k with odd k vanish as a consequence of the conservation of parity in the electromagnetic interaction. Thus, the direction of nuclear polarization cannot be detected by measurement of only the angular distribution, $W(\theta)$, of the γ rays, since the distribution is the same for both polarized and aligned nuclei. The direction of polarization can be determined by measurement of a property of the γ ray that does depend upon the degree of nuclear polarization; e.g., the circular polarization of the γ ray. This measurement is rather difficult experimentally, and another property of polarized nuclei was chosen. The spatial asymmetry of β particles emitted during β decay of polarized nuclei was determined.

D. Allowed Beta Decay

The nonconservation of parity in the weak interaction[17] gives rise to a spatial asymmetry in the angular distribution of electrons or positrons produced in the allowed β decay of polarized nuclei.[18] Explicit expressions have been presented for the angular distribution as a function of the β-decay matrix elements and of the parameters that determine the mixing ratios of the interactions in the β-decay Hamiltonian.[19]

The angular distribution of β particles from polarized nuclei may be represented by a function $W(\theta)$ analogous to that defined by Eq. (3). In the β asymmetry case, however, the odd terms in the expansion must also be included. In practice, the magnitude of the asymmetry is so poorly determined that only the large $k = 1$ term is required to fit the experimental distribution. The β angular distribution is given in reference 19 as

$$W_{\pm}(\theta) = 1 + b_{\pm}\left(\frac{m}{E}\right) + \frac{\sqrt{3}}{2I}\left(\frac{v}{c}\right) A_{\pm} B_1 P_1 ,$$

where θ is the angle between the direction of electron emission and the vector I; m and E are the electron mass and energy, respectively, I is the spin of the parent nucleus before β decay, and v/c is the ratio of the electron velocity to the velocity of light. The upper sign denotes a positron distribution, and the lower sign the distribution of electrons. The functions $b_{\pm}$ and $A_{\pm}$ are analogous to the F coefficients for γ-ray decay and depend in a complicated way on the β-decay matrix elements M_F and M_{GT} which are the Fermi and Gamow-Teller matrix elements, respectively. The former gives rise to an electron-neutrino pair with antiparallel spins so that $\underset{\sim}{S} = \underset{\sim}{S}_e + \underset{\sim}{S}_\nu = 0$. This requires $\Delta I = 0$ for the decay process. The latter matrix element gives rise to parallel spins for the electron-neutrino pair so that $\underset{\sim}{S} = \underset{\sim}{S}_e + \underset{\sim}{S}_\nu = 1$. This triplet state may be formed during decays in which $\Delta I = 0, \pm 1$.

Thus, a transition with $\Delta I = \pm 1$ produces pure Gamow-Teller radiation, but a $\Delta I = 0$ transition may be a combination of Fermi and

Gamow-Teller radiations unless the decay is between states with spin 0. These coherent waves give rise to an interference term in the description of the electron asymmetry when the initial state is restricted by polarization.

Experimental evidence[18] indicates that the β-decay interaction is an admixture of only vector and axial vector interactions with no scalar or tensor components.[19] This finding allows the angular-distribution function to be simplified to give

$$W(\theta) = 1 + \frac{\sqrt{3}}{2I} \left(\frac{v}{c}\right) A_{\pm} B_1 P_1 , \tag{6}$$

where $A_{\pm}$ is now a less complex function of the decay parameters.

For pure Gamow-Teller radiation (i.e., $\Delta I = \pm 1$) $A_{\pm}$ is given by

$$A_{\pm} = \pm \lambda,$$

where $\lambda = 1$ for $I_f = I_i - 1$, and $\lambda = - I_i/(I_i+1)$ for $I_f = I_i+1$.

If $\Delta I = 0$, mixing of the Fermi and Gamow-Teller radiations may give rise to an interference term in $A_{\pm}$. Then, $A_{\pm}$ is given by

$$A_{\pm} = \frac{\pm \frac{1}{I+1} |C_A|^2 |M_{GT}|^2 - 2 \left(\frac{I}{I+1}\right)^{\frac{1}{2}} (C_V C_A^*) M_F M_{GT}^*}{|C_V|^2 |M_F|^2 + |C_A|^2 |M_{GT}|^2} , \tag{7}$$

where C_V and C_A are the coupling constants for the vector and axial vector components of the interaction, and M_F and M_{GT} are the Fermi and Gamow-Teller matrix elements for the particular nuclear decay. The magnitude of $M_F M_{GT}^*$ gives the amount of interference between the two decay processes.

Measurements of the β asymmetry from many nuclei having $\Delta I = 0$ (e.g., Co^{58} 2+ to 2+;[20] Mn^{52} 6+ to 6+;[21] Co^{56} 4+ to 4+[22]) have indicated that the interference term is generally very small. The magnitude of the asymmetry in each of these cases was given to good accuracy by assuming that the decay proceeds by a pure Gamow-Teller transition--that is, by assuming that the interference term was zero.

On the assumption of pure Gamow-Teller radiation for a $\Delta I = 0$ transition, $A_{\pm}$ is simplified to

$$A_{\pm} = \pm \frac{1}{I_i + 1} \quad . \tag{8}$$

III. EXPERIMENTAL EQUIPMENT

A. Demagnetization Cryostat

The demagnetization cryostat is shown schematically in Fig. 1. The physical arrangement of the equipment is shown in Fig. 2. A liquid helium bath was contained in the inner of two double-wall glass Dewar vessels, D. This bath provided a heat sink at about 1 °K into which the heat of magnetization of a paramagnetic salt was absorbed. While the Dewar contained liquid helium, the space between the walls was pumped continuously by an oil diffusion pump and mechanical forepump. Surrounding the helium Dewar was a double-walled Dewar containing liquid nitrogen. This protected the easily vaporized helium bath from room temperature radiation. Visual access was provided by a 0.5-in.-wide unsilvered strip down opposite sides of both Dewars. The Dewars nested very snugly together and allowed a maximum convenient working space of 1-1/16 in. diam inside the five glass walls, two vacuum spaces, and two liquid baths which fitted inside the 2-5/8-in.-wide pole gap of an electromagnet.

The central chamber, C, was a 32-mm o.d. glass tube in which the thermal-contact assembly (Sec. III-G) was suspended. This chamber could be evacuated by an oil-diffusion pump, DP, and by a mechanical pump to allow thermal isolation of the inner assembly from the surrounding heat sink. Or it could be filled to a small pressure with helium gas to allow exchange of heat with the liquid helium bath. After being mounted, this glass tube was painted with aqueous graphite to thermalize incoming radiation to the bath temperature, thereby minimizing the heat leak into the cooled assembly. The pumping tube formed a vertical loop above the vacuum chamber to stop thermal radiation from hot surfaces above the liquid level of the bath.

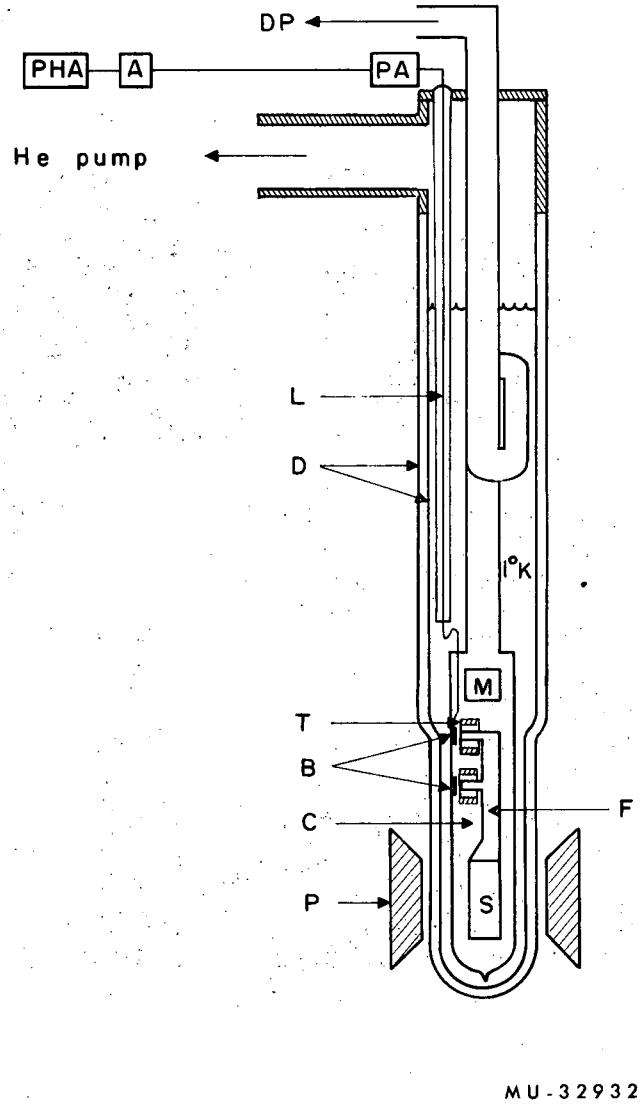

Fig. 1. Diagram of the demagnetization cryostat. The components are described in the text.

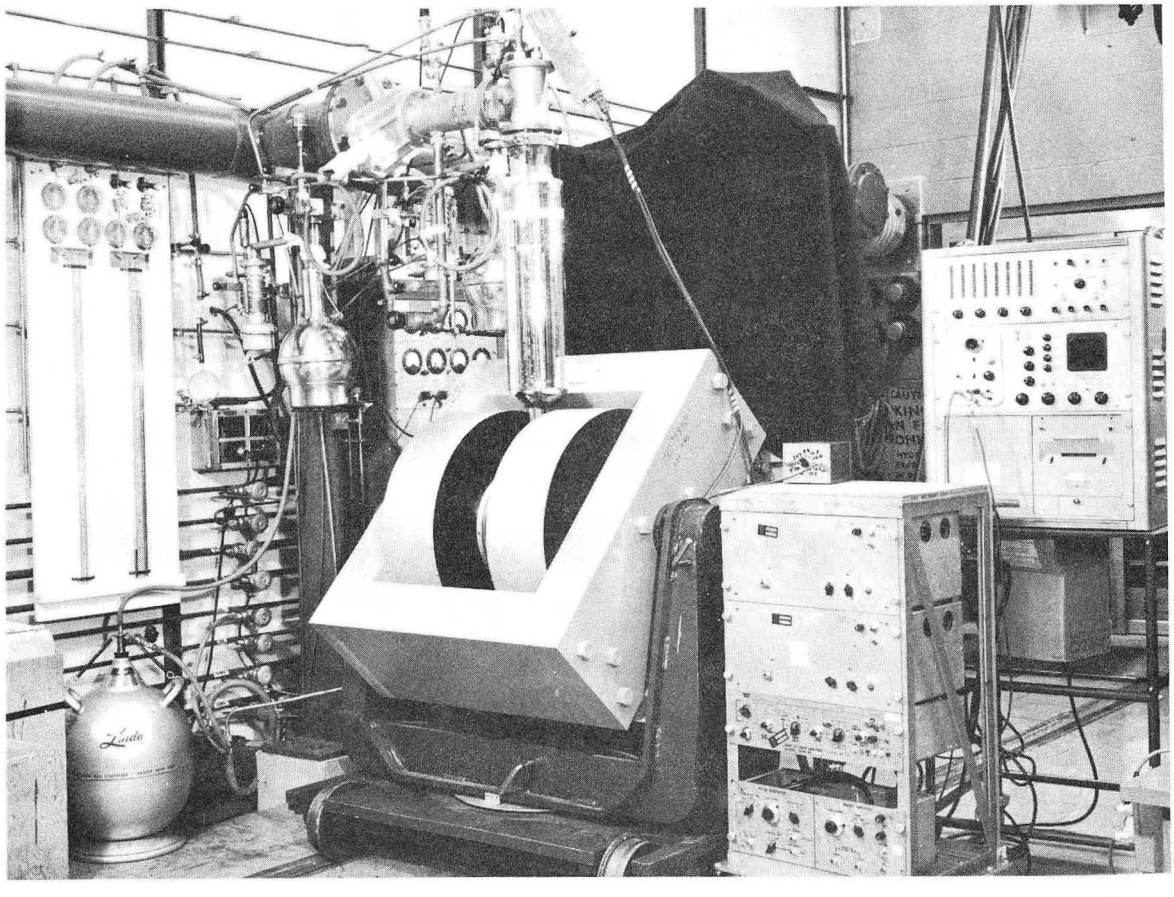

ZN-4064

Fig. 2. Arrangement of equipment during magnetization.

B. Electromagnet

The magnet used for adiabatic demagnetization was a 60-kW low-impedance H-type electromagnet that produced a maximum magnetic field of 22.0 kG in a 2-5/8-in. gap from 295 A of direct current. The pole tips, P, tapered from 12-in. to 4-in. diam over a 1-1/2-in. thickness, so the perpendicular field gradient was not large. The magnet was mounted on metal-rimmed wheels which ran on a track. It could be moved up to the Dewar position for magnetization and rolled away after demagnetization for counting and magnetic measurements on the cooled salt assembly. The polarity of the magnet could be reversed by interchanging the power cables.

Two power supplies were used for powering the magnet during the experiments to be described. The first of these was a full-wave rectified, 3-phase transformer with a transistorized regulator (Spectromagnetic Industries, Inc., Hayward, California). This unit was capable of series-regulating 300 A to 1 part in 10^5. The second dc power supply consisted of a Westinghouse induction-motor—dc-generator set capable of producing 240 A of direct current. This current did not have a high degree of regulation, however. The current ripple was greater than 1 part in 1000 without filtering and contained many high-frequency components. Joule heating of the metallic parts of the thermal-contact assembly proved to be a problem. A 70,000 μF bank of capacitors across the magnet decreased the ripple in the current to a point at which a workable minimum of Joule heating was produced. The primary function of the capacitors was to reduce the ripple frequency, which in turn greatly reduced the eddy-current heating. The magnet has a self-inductance of 2/3 H and a dc resistance of 2/3 Ω. Thus, its 1-sec time constant also aided in attenuating the high frequencies.

C. Magnetic Thermometer

The temperature of the paramagnetic salt was monitored after demagnetization by means of the temperature dependence of its magnetic susceptibility. The susceptibility was determined by measuring the voltage induced into the secondary of a coaxial coil pair surrounding the salt. The voltage from this secondary coil was compared to the voltage from the secondary of an identical coil pair which did not contain any paramagnetic material. These coil pairs were wound with No. 40 (B and S gauge) formvar-coated copper wire and were both located in the helium bath one above the other. Figure 3 shows the coils in place on the glass cryostat. The two secondary voltages were compared by the null method. Sufficient additional voltage was added externally to cancel the small difference in the output of the two cryostat coils. The mutual-inductance bridge built for this purpose allowed the simultaneous adjustment of the amplitude and phase of a 20-cycle induced voltage.[23] The net voltage was then amplified and viewed with the vertical plates of an oscilloscope while the primary voltage was fed to the horizontal plates. An elliptical pattern resulted when the circuit was out of balance. A null was obtained by adjusting the amplitude and phase of the bridge output until a horizontal line appeared on the oscilloscope. The bridge reading then gave the net inductive difference of the two secondary coils. This reading is proportional to the susceptibility of the salt.

D. Radiation Detectors

1. Gamma Counters

Two identical γ-ray counters were used. These were scintillation counters utilizing 3-in.-diam by 3-in.-long NaI(Tl) crystals optically mounted onto Dumont 6363 photomultiplier tubes. The phototubes were coupled to the amplifier circuits by White cathode-follower preamplifiers. The pulses were amplified by double-decay-line pulse amplifiers and then separated according to height by a transistorized 256-channel pulse-height analyzer (Technical Measurements Corporation, North Haven, Conn.). Normally, one of these counters

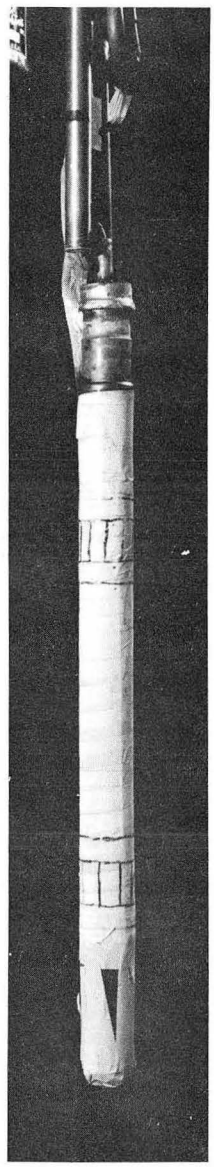

ZN-4066

Fig. 3. Two coaxial-coil pairs mounted on the glass cryostat. The lower set contained the paramagnetic salt; the upper pair contained no paramagnetic material. The windings are covered with tape to prevent movement and damage.

was placed along the magnetizing axis and the other placed perpendicular to the axis as shown in Fig. 4.

2. Beta Counter

A germanium surface-barrier counter was used for the detection of beta radiation. It was placed inside the glass cryostat and received radiation emitted along the magnetizing axis. The counter is located at B in Fig. 1. The counter was originally developed for low temperature alpha counting,[24] and an improved design[25] gave good electron resolution (see Sec. VI-C).

The lead wire, L, for the beta counter was brought into the helium bath through a separately pumped tube. The wire emerged from the bottom of this tube at a Kovar seal and continued through the helium bath in an S curve and into the cap of the vacuum chamber through another seal. In the long passage of the wire down the tube into the helium bath, care was taken to minimize capacitive effects by stretching the wire down the center of the tube.

A preamplifier, PA, was placed immediately outside the upper end of this tube. A linear pulse amplifier, A, was connected to the preamplifier by shielded cable.

Because of the very small output pulse heights of the detector, an amplification factor of more than 10^6 was required. The amplified pulses were separated by the pulse-height analyzer, PHA, and recorded.

E. Polarizing Magnet

The magnet used to polarize the ferromagnetic alloys to saturation consisted of a short tube of pure niobium, which is a superconductor under the experimental conditions. The tube, T, was made to trap part of the field produced by the electromagnet. The temperature of the tube remained near 1°K, well below the 9.2°K zero-field superconducting transition temperature. Upon magnetizing at 1°K, a field was reached at which the superconducting niobium became a normal metal. The niobium remained normal as the field was

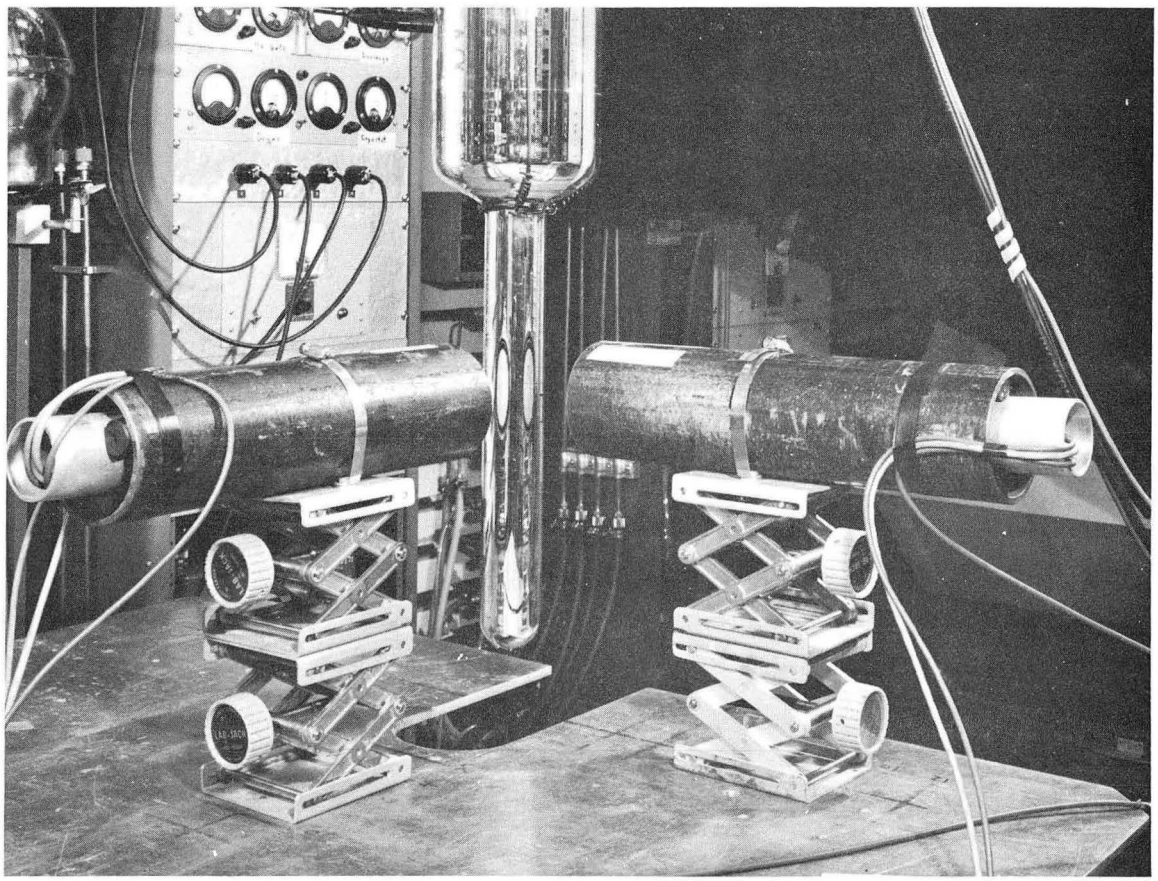

ZN-4065

Fig. 4. Gamma-ray scintillation counters in magnetic shields. The right-hand counter is parallel to the magnetization axis.

further increased. During demagnetization, the field was slowly removed until the niobium again became superconducting at this same critical field. At this point a supercurrent was set up within the niobium which produced a magnetic field in the tube equal to the critical field. The external field was then removed completely, leaving the current and field trapped in the niobium tube.

The tube was cut from a rod of electron-beam-refined niobium metal, annealed for 2 hours in vacuum at 1250°C, copper plated, and soldered onto a brass holder. It was placed with the axis of the tube parallel to the magnetic field of the electromagnet. In this position the magnetic field set up by the current in the niobium also lay parallel to the axis of the electromagnet.

The dimensions of the tube were determined by the size of the field desired. Tubes with several wall thicknesses and various lengths were prepared and the maximum fields measured at 4.2°K with a rotating-coil probe. These fields are shown in Fig. 5. The tube chosen for these experiments was 1/2 in. o.d.× 3/8 in. i.d. ×3/8 in. long and held a field of 2300 G at its center. The field profile was such that the field near the ends of the tube was more than 75% of the field at the center. The sample was always kept within the central portion of the tube and on the tube axis. The field varied less than 10% from the maximum across the alloy sample, and was sufficiently high to produce essentially 100% saturation in the iron and nickel alloys.

The field along a line perpendicular to the axis and through the center of the tube was also important. This fringing field was found to be only of the order of the earth's field at about 2 in. away from the center of the tube. This dimension was important for construction of the thermal-contact assembly described in Sec. III-G.

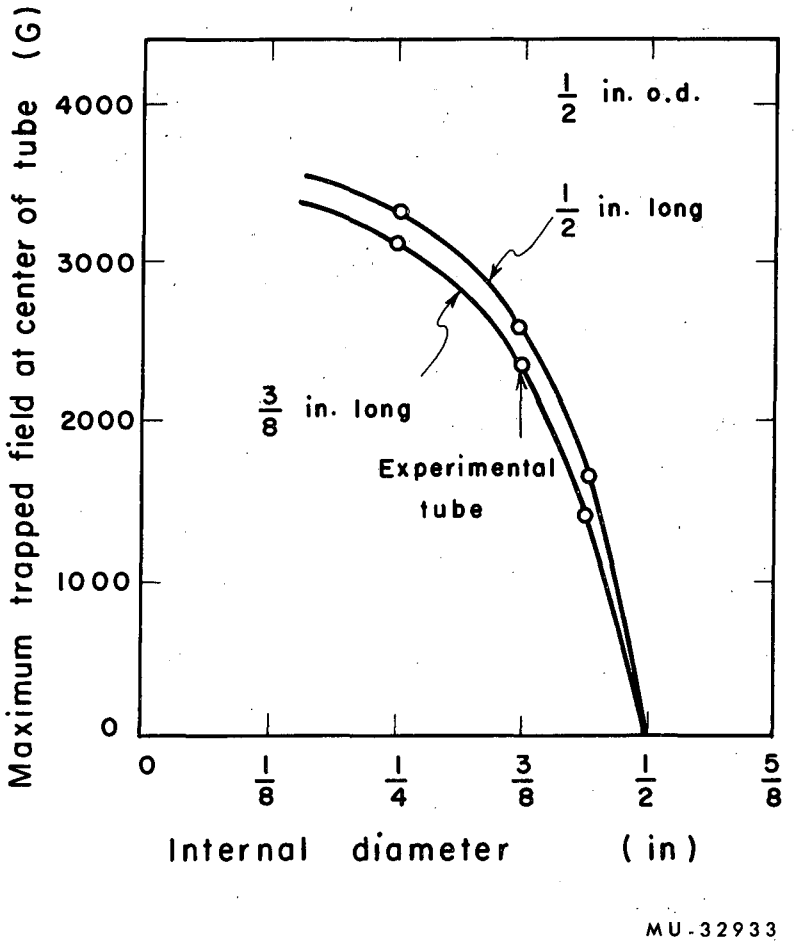

Fig. 5. Maximum trapped magnetic fields in niobium tubes as functions of tube dimensions. The tube used for these experiments was 3/8 in. i.d. × 3/8 in. long, and is indicated by the arrow.

F. Alloy Preparation

All alloys used in these experiments were prepared in essentially the same way. The metals were placed in a small-diameter short quartz tube which was sealed at one end. This tube was then inserted into a long quartz tube and the assembly was flushed with argon for several minutes. A long narrow glass tube was filled with argon and inserted with a stopper into the top of the large tube so that it added several feet to the overall length. This provided a long narrow path to slow air diffusion down into the melting zone. Bright metallic alloy melts were always obtained in this way.

This quartz assembly was lowered into a preheated electric resistance furnace which was heated by a Kanthal element. The maximum temperature attainable was 1600°C. This is 65°C above the melting point of iron, the highest melting material used. The alloy was left in the furnace for approximately 10 minutes and then slowly removed.

Several iron-silver and nickel-silver alloys were prepared in this way. Typically, 1 g of ferromagnetic metal in the form of wire and a 0.1-mg piece of radioactive silver was used for each alloy. These were first melted together in the furnace. The melt was then cut into several pieces with a chisel and hammer. The homogeneity of the alloy was determined by weighing and counting the activity of each piece. No alloy was ever found to be inhomogeneous within the accuracy of the weighing (10^{-4}g).

Because of the high vapor pressure of molten silver at 1600°C, much of the silver was volatilized and remained on the quartz tubes. While the initial composition of the mixture was normally 0.01% silver, the final composition after melting was approximately 0.001% silver. The composition could easily be adjusted by varying the length of time in the furnace.

The solubility of silver in iron is reported[26] to be less than 2×10^{-3}% while the solubility limit in nickel is known[27] to be greater than 3.6%. Very dilute alloys of silver in iron were therefore required.

Experiments were performed with alloys of two compositions. These were 0.001% silver in iron and 0.0005% silver in iron. The second composition was used to experimentally verify the complete solubility of silver in both alloys. Only one composition of silver in nickel was used, and it contained 0.01% silver.

Radioactive Ag^{110m} was produced by neutron irradiation of natural silver metal. The metal foil was cut into several 0.1-mg pieces, sealed in a quartz tube, and irradiated with thermal neutrons. The nuclear reaction is $Ag^{109}(n, \gamma)\ Ag^{110m}(253d)$.

A high specific activity of Ag^{110m} was required because of the need to dilute the active metal with considerable inactive material in preparing the experimental alloys. A one-week irradiation with the high neutron flux of the General Electric Company reactor at Vallecitos, California was sufficient for preliminary experiments. Another source of Ag^{110m} was later obtained from Oak Ridge National Laboratory. It contained 21 curies of Ag^{110m} per gram of silver and represented a 27-fold increase in specific activity. This nitric acid solution was used for electroplating additional active silver onto the iron-silver alloys described above. The alloy was then remelted in the furnace only sufficiently long enough to allow diffusion to occur. The activity of the alloy was thus greatly increased without significant change in composition. These more active alloys were used for all quantitative experiments.

G. Thermal-Contact Assembly

The radioactive-metal alloy must simultaneously be magnetized to saturation and cooled to a temperature of a few hundredths of a degree Kelvin. This was accomplished by means of the thermal-contact assembly to be described below. This assembly was the most important piece of apparatus developed during the course of this work and its final design was the result of many trials.

The alloy was cooled by thermal contact with a paramagnetic salt, chromium potassium sulfate, which could be cooled to near 0.01°K by adiabatic demagnetization. The salt had to be kept near

this temperature long enough to allow thermal equilibrium with the alloy to be established. The equilibrium temperature could not be higher than a few hundredths of a degree or no appreciable nuclear polarization would occur. Also, the warming rate of the alloy had to be sufficiently slow to allow time for statistical accuracy in the counting processes used for detection of the polarization.

The requirement that a magnetic field of a few thousand gauss be placed on the alloy precluded direct physical contact between it and the paramagnetic salt. Adiabatic demagnetization of a typical paramagnetic salt from a field of 25 000 G to a field of 2 500 G reduces the temperature of the salt from 1°K to approximately 0.1°K.[28] Only complete removal of the field will cool the salt to the order of 0.01°K. Thus, if the salt remained in even a small residual magnetic field, the required temperature could not be reached. It was for these reasons that a thermal link between the salt and the alloy had to be introduced. The link had to be long enough so that the magnetic field at the salt would be negligible. Its length therefore depended on the geometry of the polarizing field. Along with the link, however, was introduced the additional requirement of thermal contacts between the salt and the link and between the link and the alloy. A detailed description of these two contacts is given below.

Copper was used for construction of the link, since its thermal conductivity is known to be sufficiently large in this temperature range.[29] Thermal links of both small diameter copper wire and thin copper foils have been reported.[30] Copper foils have the advantage of structural stability in two dimensions rather than in one and are considerably easier to handle than wires. For these experiments, twenty-five 5-mil copper foils were cut into the shape shown at F in Fig. 1. Each of these was annealed with a cold flame and cleaned in acid. They were then stacked one on the other and the upper ends soldered together with silver solder. Care was taken to assure that the solder penetrated between the foils and down to within 1/2 in. of the rectangular end. The total fin assembly weighed about 70g and had

an exposed surface area of more than 800 cm^2. The completed fin assembly is shown in Fig. 6. The glass casing which held the salt and fins is also shown. Above the case is one of the germanium β counters.

The upper end of the fin assembly had two rectangular snouts protruding from the vertical foils. These protrusions were, however, an integral part of each foil. The snouts were sanded flat on the bottom so that each foil could be seen clearly. The flattened alloy was soldered onto the bottom of one snout with Pb-Sn solder. Every effort was made to make this solder layer as thin as possible. All excess solder was then filed off and the alloy surface sanded clean. The alloy thickness was usually 5 mils or less. The alloy was soldered to the bottom of the snout in such a position that it would lie in the center of the niobium tube without the tube touching the snout or the vertical part of the link. After an experiment was completed and the alloy removed, all the old solder was removed from the snout and the surface again made smooth. In this way the foils were used again and again.

Chrome alum [$CrK(SO_4)_2 \cdot 12\ H_2O$] was chosen as the paramagnetic salt because of its high heat capacity at low temperatures[31] and because it may be cooled to 0.01°K from the initial temperature and magnetic field available. Also, the relation between the thermodynamic temperature and the magnetic susceptibility has been reported.[32]

Thermal contact between the copper link and the chrome alum was achieved in the following way. The salt was ground to a fine powder and made into a thick slurry by mixing it with a solution containing 50% saturated salt solution and 50% glycerine by volume. The usual proportions of these used in the slurry were 12 g of salt to 5 g of solution. The actual composition was determined by the consistency of the slurry.

The slurry, which is shown at S in Fig. 1, was spread onto one side of each fin and the resulting multilayer sandwich placed inside the thin-walled glass casing. The empty space remaining inside

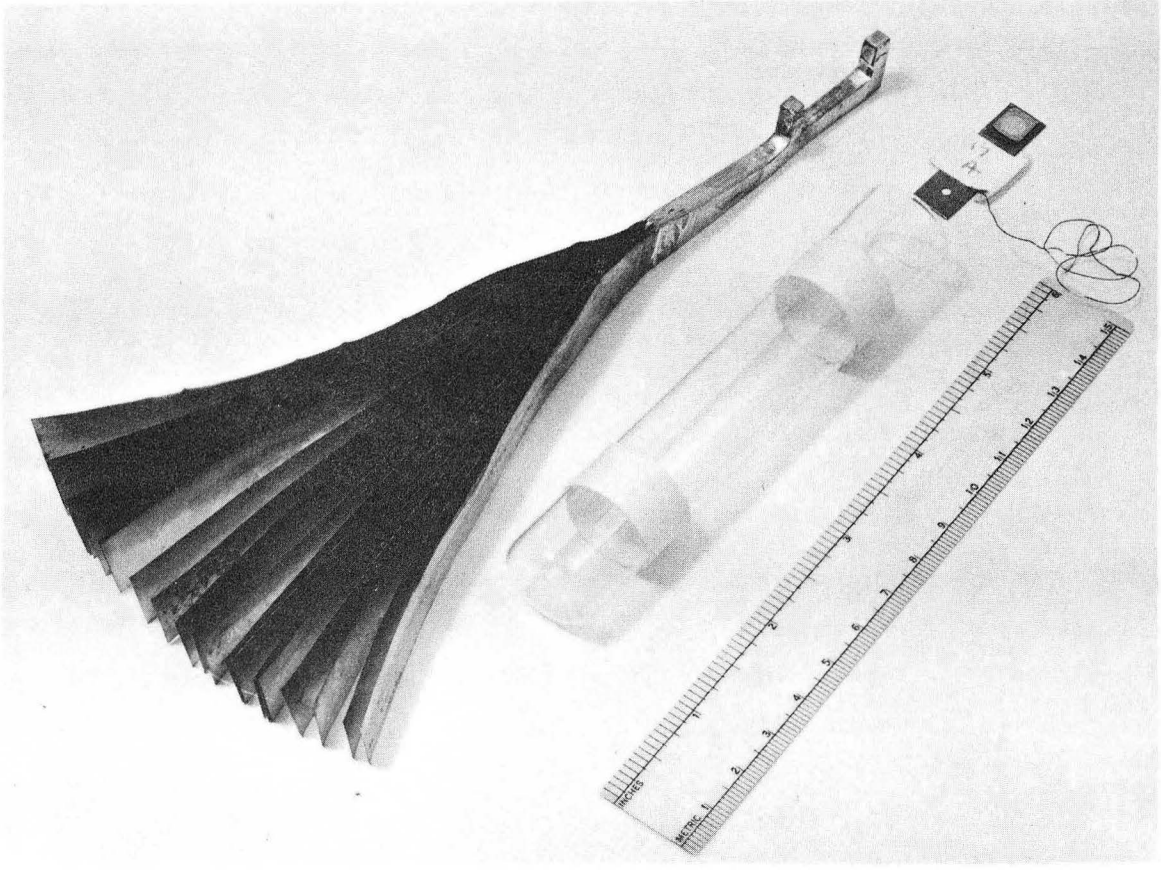

ZN-4069

Fig. 6. Copper-fin assembly showing snouts on the upper end and the large surface area for contact with the paramagnetic salt. The thin-walled glass case held the salt around the fins. A low-temperature germanium β counter is shown above the case.

the casing was then filled with additional slurry. The assembly contained approximately 60 g of slurry of which more than 40 g was powdered chrome alum. The case was wrapped at two places with porous adhesive tape to facilitate its mounting in the cryostat.

The assembly was suspended in a brass cage by six plastic threads of about 10-mil diam stretched under spring tension inside the cage. The assembly was held in position by tying a piece of thread around the strings and the glass case at each of the two tapes. The assembly was mounted in the cage; the suspension was then carefully scrutinized to determine whether the glass case or the upper snouts of the fin assembly touched the brass cage or the magnets, which would remain at about 1°K. After careful adjustment, the assembly was fixed in place by gluing the threads to the tape at each thread intersection, with fast drying cement.

Above the assembly was placed a pressed pill of manganous ammonium sulfate. This paramagnetic material was also magnetized by the fringing field of the electromagnet, and upon demagnetization served as a cold surface for absorption of warm gas that might enter the chamber from above. The pill, which was a 3/4-in.-high cylinder, covered more than 50% of the cross section of the cryostat tube and is shown at M in Fig. 1. The completed suspension is shown mounted inside the cryostat in Fig. 7. A closeup photograph of the arrangement of the snouts and magnets is shown in Fig. 8. Behind the upper magnet is the sensitive surface of the β counter.

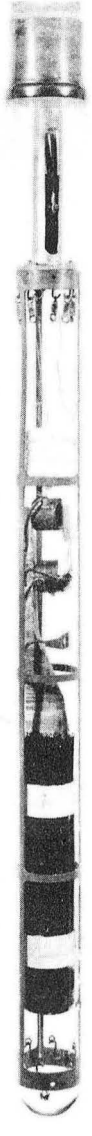

ZN-4067

Fig. 7. Thermal-contact assembly suspended by threads in a brass cage; the cage is mounted inside the glass vacuum chamber.

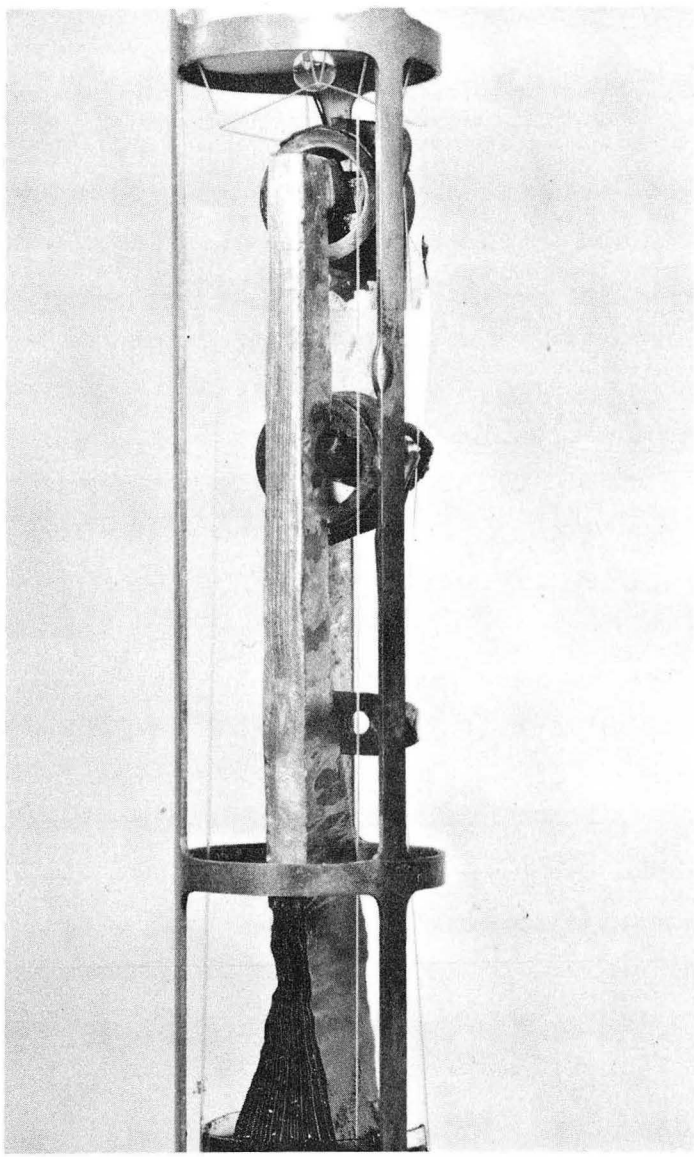

ZN-4068

Fig. 8. Relative position of fin-assembly snouts and niobium tubes. A β counter is mounted behind the upper tube. The suspension threads and top of salt case may also be seen.

IV. EXPERIMENTAL PROCEDURE

The alloy to be investigated was prepared as described in Sec. III-F. It was flattened and soldered to the fin assembly. Only about 25 mg of alloy was used for an experiment. This indicates the need for a high specific activity. The paramagnetic salt slurry was prepared and smeared onto the fins. The completed thermal-contact assembly was glued into the cage and the cage was bolted onto the cap of the cryostat. The β-counter wire was connected and the cryostat tube was soldered into place. Liquid nitrogen was placed inside the helium Dewar, while a pressure of helium gas of more than 1 atm was maintained in the cryostat tube for heat exchange with the boiling nitrogen. When the slurry was placed in nitrogen within 3 hours after preparation, satisfactory cooling characteristics were obtained. Old slurry was found to warm up exceedingly rapidly after demagnetization. This was presumed to be caused by dehydration of the salt by the glycerine solution on long standing at room temperature. No study of the shelf-life of the slurry was made. Fresh slurry was prepared for each experiment. The cryostat was kept pressurized with helium gas for at least 1/2 hr to ensure that the slurry was completely frozen before pumping began. It was found that 20 min was insufficient to prevent bubbling of the slurry, which caused the fin assembly to rise and touch the niobium tube.

Pumping of the cryostat tube at 77°K was continued for several hours and usually overnight. The liquid nitrogen was then blown out of the helium Dewar through a tube inserted from the outside for this purpose. The vacuum space of the helium Dewar was then pressurized to 3 cm Hg with nitrogen gas and the remaining liquid nitrogen allowed to boil away. The outer Dewar was still empty at this time. The helium Dewar wall space was again reevacuated and the precooled Dewar filled with about 5 liters of liquid helium. Helium exchange gas was added to the cryostat during the transfer of the liquid.

Calibration of the magnetic thermometer was begun by balancing the voltage from the mutual inductance of the coils around the cryostat

with the calibrated coils of the mutual-inductance bridge. A balance was achieved at several temperatures as the liquid helium bath was cooled by pumping. The thermodynamic temperature corresponding to the bridge reading was determined by the vapor pressure of the boiling helium as measured by a mercury or oil manometer system. A plot of the mutual inductance vs 1/T yields a straight line in this temperature region because the chromium ion is nearly an ideal paramagnetic ion and thus obeys Curie's law. The helium bath could be pumped to a pressure corresponding to 0.93°K.

The paramagnetic slurry was then magnetized and the helium exchange gas was pumped from the cryostat. The magnetic field was then removed. The course of demagnetization depended upon the source of power to the magnet. When the transistor-regulated supply was used, the high regulation allowed extremely slow demagnetizations to be performed. The longest were 20 minutes. This was desirable because (a) thermodynamic reversibility would be maintained and the lowest possible temperature would be reached, and (b) Joule heating of the metal fin assembly would be minimized. Even rapid demagnetization produced negligible heating if high regulation was maintained during reduction of the field.

The motor generator set required another course of demagnetization, however. The dc output of the motor-generator set contained considerable (2%) ripple component. The capacitor filtering circuit stabilized the dc level to about 1 part in 1000 and removed the high-frequency components. This was still found to warm the sample assembly unless care was taken to minimize the heating at each stage of demagnetization. The field was brought down from 20 000 G to near 2000 G in about 1.5 min. The heat capacity of the salt in the field is much greater than the eddy-current heating; therefore, little temperature error occurred. The field was not held at this value but immediately dropped rapidly to a minimum (not zero). This allowed a minimum of ripple heating with a tolerable amount of heat caused by the rapid reduction of the field. The motor generator was now turned off and allowed to coast to a stop. The residual

magnetism of the windings of the generator caused it to produce current as long as it revolved. Rolling the magnet away from the cryostat or breaking the circuit to the magnet while the generator was in motion served only to warm the cooled assembly well above a usable temperature. This was presumed to be caused by eddy-current induction in the fins.

After demagnetization and removal of the magnet, the γ-ray counter table was rolled up to the Dewars. Magnetization of the alloy had occurred automatically during the demagnetization process. Either γ ray or β counting was begun at about 3 min after complete demagnetization. The alloy temperature as determined by the magnitude of the γ-ray anisotropy reached a minimum in this time period. Equilibrium was always very rapidly established.

During the counting period, the salt temperature was monitored by balancing the inductance bridge. The primary coils were kept disconnected between bridge readings to avoid heating the metal sample, by induction from the alternating magnetic field.

Usually a series of counting periods was recorded as the alloy slowly warmed up. Because the metal sample was only of the order of 5 mils thick, and because metals are generally good thermal conductors, temperature inhomogeneities are not present as would be the case with a poor thermal conducting material.

After a series of "cold" counts, the entire assembly was warmed to the bath temperature by addition of helium gas to the cryostat. The bridge was again balanced to ensure that complete warming had occurred. Several "warm" counts were then taken before the counters were moved away for normalization of the counting rate to the isotropic value at this geometry.

V. THERMOMETRY

A. Magnetic Thermometer

For nuclear polarization experiments to yield values for nuclear parameters, the absolute temperature of the polarized system must be known. The most widely used thermometer for this temperature range is the magnetic-susceptibility thermometer.

It is possible to measure the temperature of a spherical single crystal of paramagnetic salt to good accuracy by this method, if the magnetic properties of the salt are known. For chrome alum, the required properties have been reported for single crystals,[31, 32] but for the salt slurries used in these experiments, the magnetic thermometer is affected by the powdered state of the salt and the cylindrical shape of the slurry. Each of these geometric factors contributes a correction to the susceptibility through the demagnetizing field. The correction for the shape may be simply made, but the correction for the particle size and shape in the powder may only be approximated. For this reason an empirical relation between the susceptibility and the temperature of the slurry was established. This possibility was complicated by the fact that a fresh slurry was required for each experiment. Different slurries thus contained different particle-size distributions and had different filling factors and different magnetic properties. This was shown to be the case experimentally. The magnetic susceptibility determined immediately after demagnetization of different slurry assemblies from the same initial conditions varied considerably. Successive demagnetizations of the same slurry, however, yielded quite reproducible susceptibility measurements.

Entropy data were used to establish a relation between T, the absolute thermodynamic temperature, and $T^{\circledast}$, the magnetic temperature for a spherical single crystal of chrome alum.[31, 32] The magnetic susceptibility, and, therefore, the magnetic-temperature function, $1/T^{\circledast}$, rises to a maximum as the salt warms through the

Curie point. For a single crystal, this maximum is quite sharp and the susceptibility drops precipitously as the temperature increases. The magnetic temperature of the slurry assemblies showed this effect also, but the maximum was lower and broader than the single-crystal curve. A typical warming curve is shown in Fig. 9. The broadening may have been due to a lack of thermodynamic equilibrium within the slurry or may be inherent in the particle-size distribution in the slurry. The maximum was lowered by the demagnetizing factors mentioned. above. Normalization of the experimental curve for the slurry to the single-crystal data accounted empirically for the unknown demagnetizing factors. The temperature scale thus obtained was considered to be reliable to about 1 millidegree at the lowest temperature. The scale was based, however, on the reported value of the Curie point for chrome alum (0.0115°K), which is somewhat uncertain.

At best, the magnetic thermometer would give an accurate determination of the slurry temperature, while the temperature of the alloy was the required quantity. The magnitude of the temperature gradient along the thermal link between the slurry and the allow provided a further uncertainty in the alloy temperature. A direct measurement of the alloy temperature was therefore desirable. Fortunately, this was made possible by use of the internal radioactive thermometer described below. This thermometer allowed observation of the temperature difference between the two parts of the assembly. Figure 10 shows the results of demagnetization of several slurry assemblies. This figure shows the alloy temperature as determined by the radioactive thermometer plotted against the magnetic temperature of the slurry measured during each counting period. The solid curve is the normalized curve for the absolute temperature of the slurry. The main features to be noted are the differences among the various slurry assemblies and the difference between the experimental alloy temperature and the predicted slurry temperature. This difference amounts to about 3 millidegrees and may be the result of a thermal gradient between the alloy and the slurry or of an error in the accepted value of the Curie point.

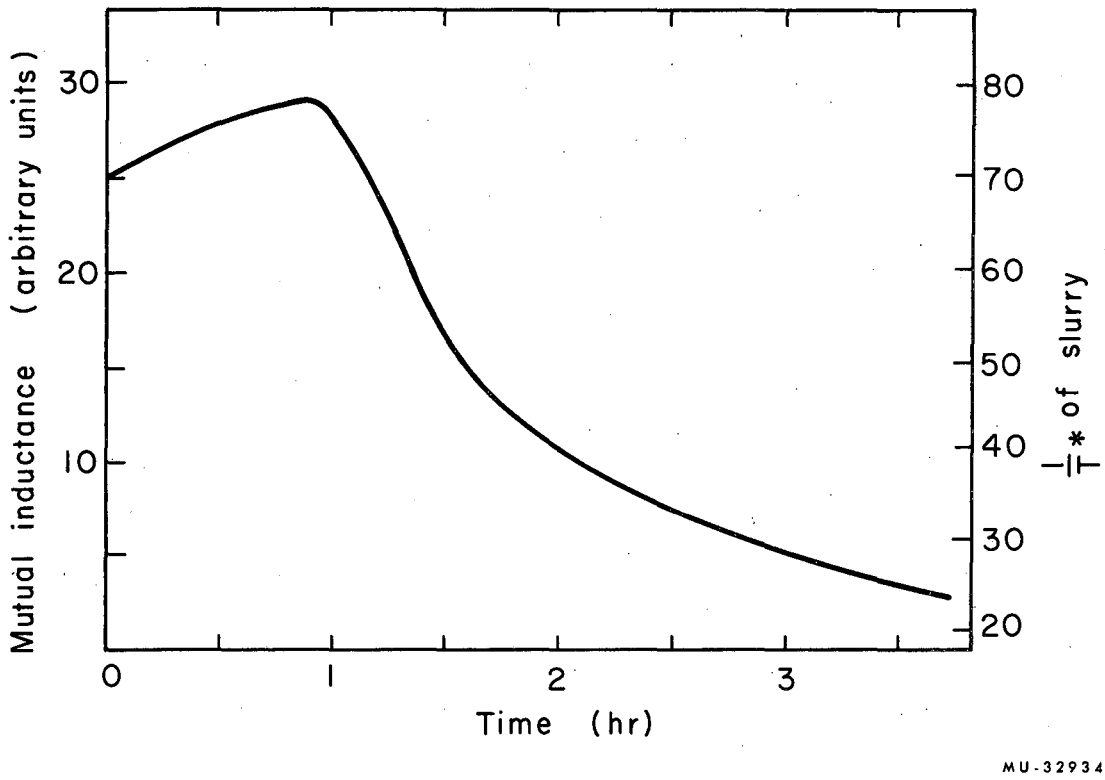

Fig. 9. Warm-up curve for chrome-alum slurry and fin assembly. The maximum susceptibility occurs just below the Curie temperature.

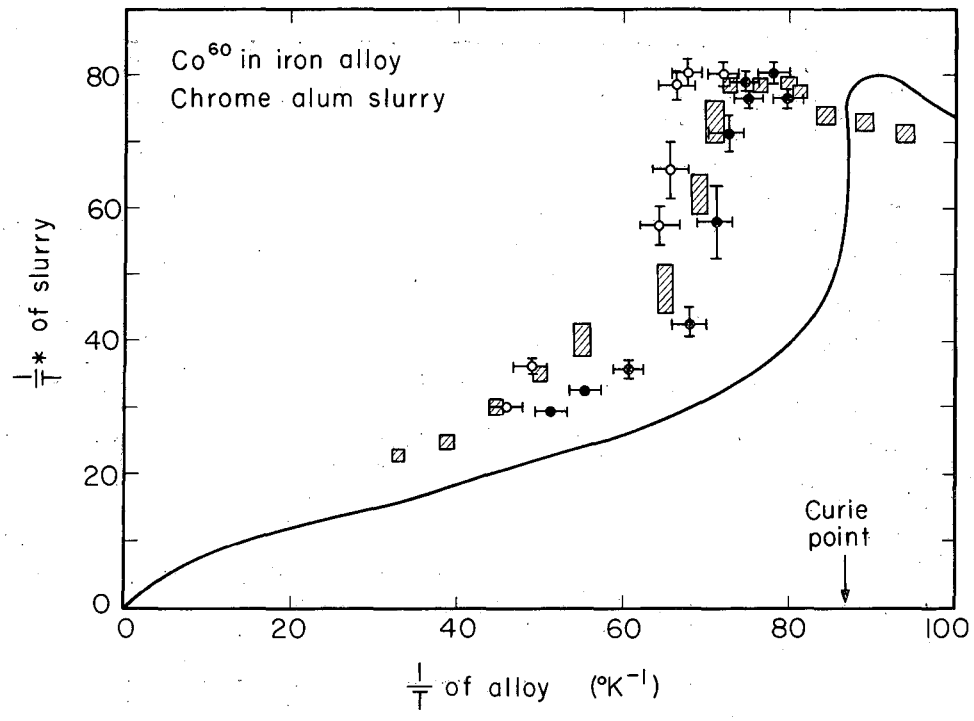

Fig. 10. Plot of alloy temperature against magnetic temperature of salt slurry. Solid curve is predicted salt temperature. Variation of experimental points is due to thermal-contact variation and radioactive heating.

B. Co^{60} Thermometer

The nuclear parameters of Co^{60} are well known and allow calculation of the temperature dependence of the angular distribution of γ radiation from Co^{60} polarized in iron. The nuclear spin, $I = 5$, magnetic moment, $\mu = +3.80$, and the internal field at cobalt in iron,[33] $H = 289.7 \times 10^3$ G, allowed calculation of B_2 and B_4 as functions of temperature. The two γ transitions in Co^{60} are pure E2; thus F_2 and F_4 were known for each: $F_2(1172) = -0.448$ and $F_2(1333) = -0.598$. Also, U_2 and U_4 may be calculated exactly, since the 5+ to 4+ β transition is pure Gamow-Teller radiation. Calculation gave $U_2(1172) = +0.898$ and $U_2(1333) = +0.673$ and, furthermore, $U_2F_2(1172) = U_2F_2(1333) = -0.402$. The term with $k = 4$ was also calculated and $W(\theta)$ determined. The γ-ray angular distribution was thus exactly known as a function of temperature. The calculated value of $W(0)$ vs $1/T$ is shown in Fig. 11. $W(0)$ has been normalized to unity at high temperatures. In the figure the term $k = 4$ has been included separately to show that, while small, it is not negligible at the lowest temperature. This curve is valid for either of the γ rays from Co^{60}. The experimental value of $W(0)$ for Co^{60} polarized in iron was used to determine the temperature of the alloy. Several experiments with Co^{60} in Fe were performed to check the contact-cooling assembly. A typical γ-ray spectrum of Co^{60} polarized in iron is shown in Fig. 12. The temperature of the alloy in this case was 0.015°K.

The establishment of the temperature of the alloy allowed a more positive study of the thermal conductivity of the two thermal contacts. The primary considerations were determination of the time required for the alloy to cool to the minimum temperature and the magnitude of this equilibrium temperature. Figure 13 shows the experimental anisotropy of Co^{60} as a function of time after demagnetization. It is clear that the establishment of equilibrium was rapid and occurred within the first few minutes after the end of demagnetization.

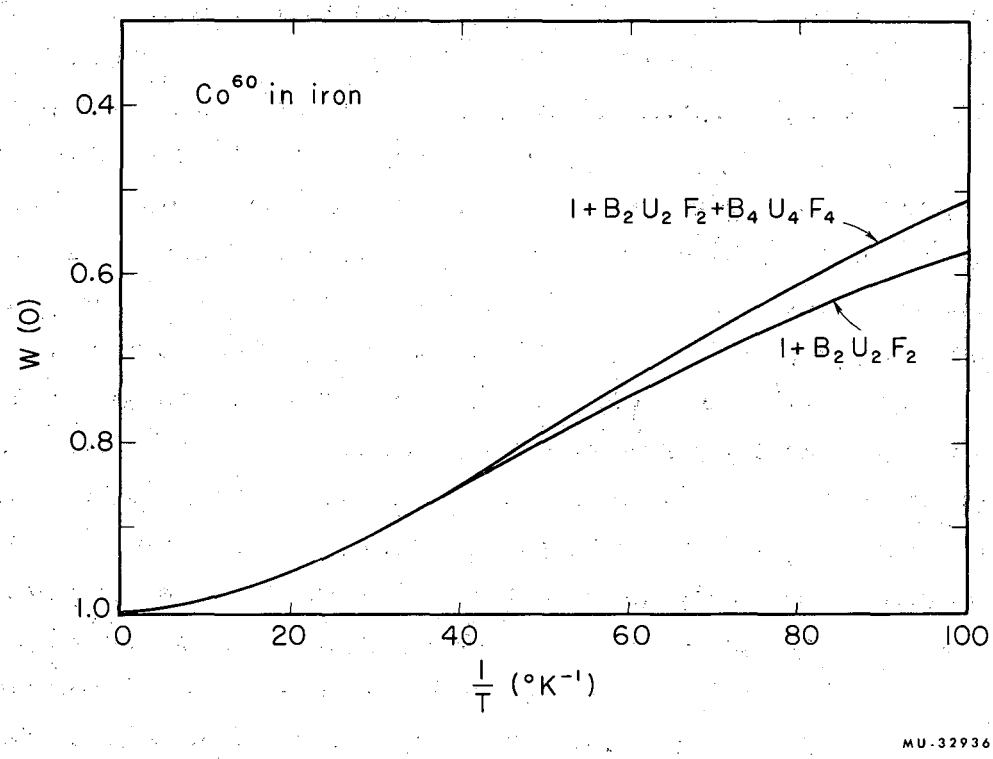

Fig. 11. Calculated angular-distribution function, W(0), for Co^{60} in iron as a function of 1/T.

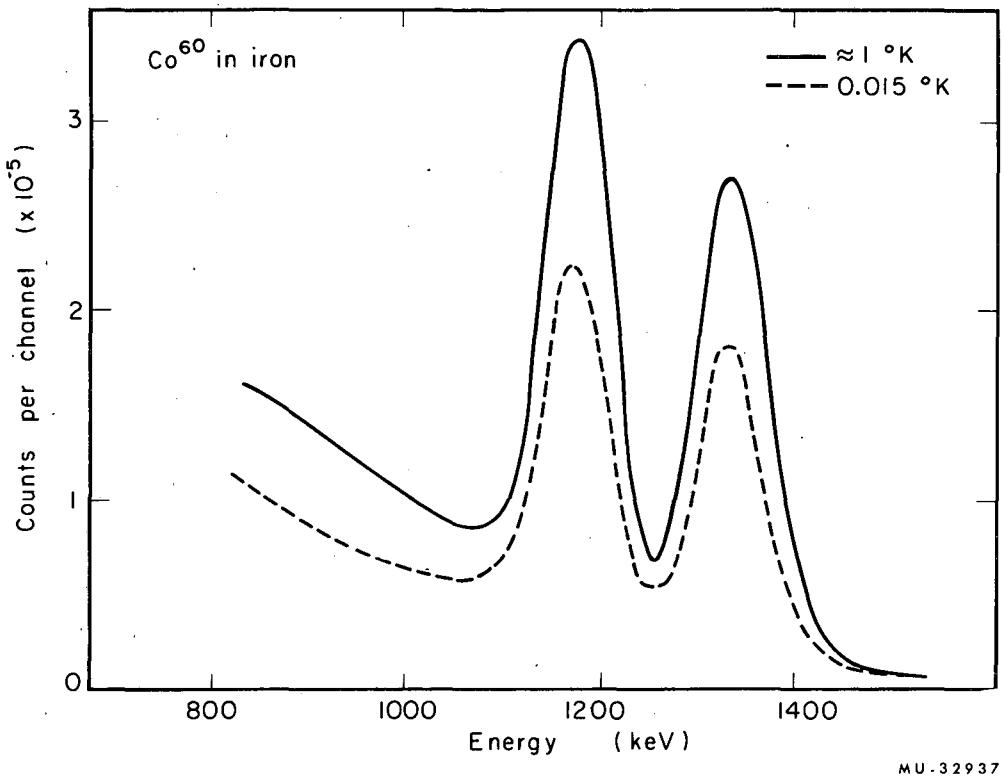

Fig. 12. Gamma-ray spectrum of Co^{60} polarized in iron at 0.015°K (dashed curve) and about 1°K (solid curve). This spectrum was taken along the magnetization axis at $\theta = 0$.

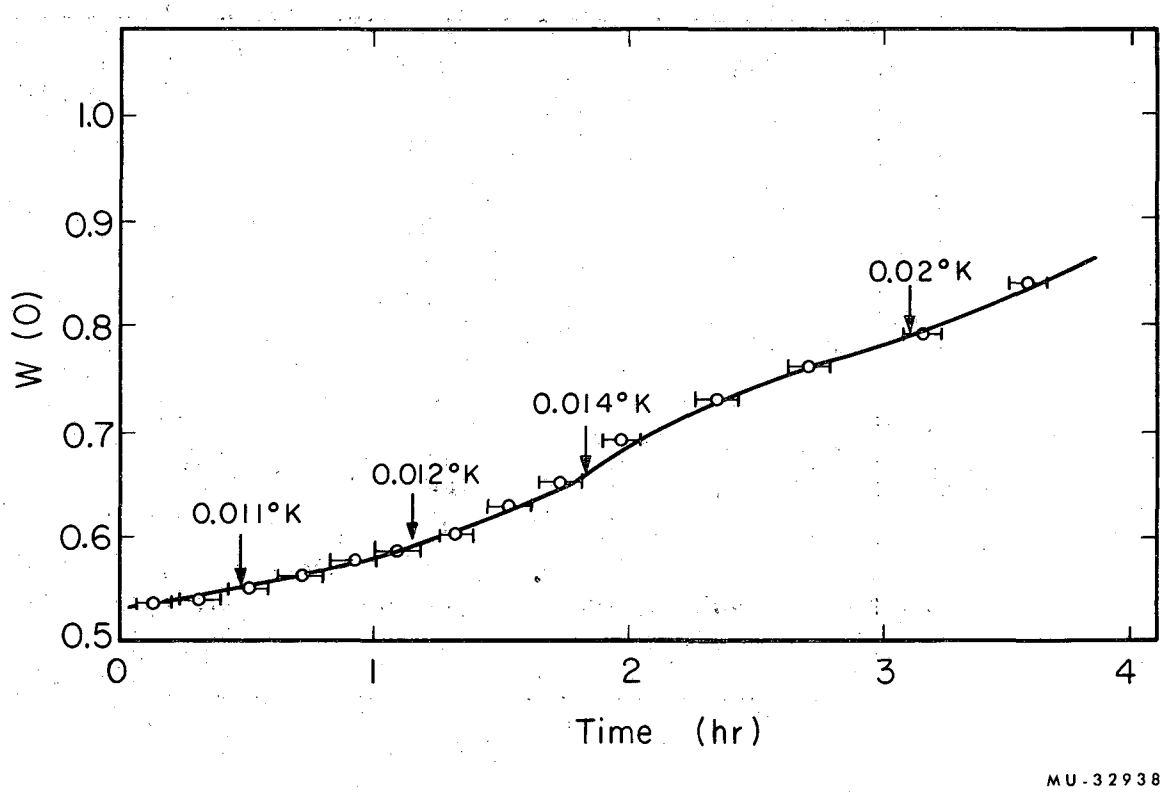

Fig. 13. Magnitude of W(0) for Co^{60} in iron as a function of time after end of demagnetization. Temperatures shown were read from Fig. 11.

The minimum temperature reached was 0.0105°K. The alloy warming rate was only 30 microdegrees per minute during the first hour of warmup and slowed after that because of the increase of the heat capacity. The slow warming rate indicated that long counting periods could be used without significant change in the temperature. Thus, radioactive heating of the alloy was negligible.

In the initial stages of this work the temperature scale for Co^{60} in nickel was calculated by using the only value of the hyperfine field that had been determined. This value was 80 kG and was obtained by a rather questionable extrapolation of the nuclear heat capacity[34] of quite concentrated alloys of cobalt and nickel. The lowest temperature determined by use of dilute alloys of Co^{60} in iron already described indicated that the minimum temperature attainable with the thermal-contact assembly was about $1/T = 95$. The magnitude of W(0) measured for several alloys of Co^{60} in nickel indicated that the temperature would have to be well below 0.01°K to yield the large values of W(0) observed. The field at Co^{60} in iron was determined by a resonance method, and is thus accurately known. Because the field is known and because $1/T = 95$ is about the minimum temperature obtainable by demagnetization of chrome alum from the experimental conditions, the value of 80 kG for Co^{60} in nickel was abandoned in favor of a higher value. Using $1/T = 95$ and the experimental W(0), the value H = 120 kG was obtained. This value was established without knowledge of a recent nuclear magnetic resonance (NMR) measurement of this field.[35] The value obtained by NMR was 112.7 kG at 27.4°C. Correction of this value to 0°K yielded 119.9 kG!

The polarization data are not this accurate, however, and the agreement is fortuitous. Nevertheless, this prediction established the validity of the temperature scales for Co^{60} in both iron and nickel and greatly increased confidence in the ability to accurately determine the alloy temperature from W(0) for Co^{60}. The final temperature scale for Co^{60} in nickel is shown in Fig. 14. The term with $k = 4$ is seen to be very small for this alloy, since the hyperfine field is small. This curve is valid for either of the two γ rays from Co^{60}.

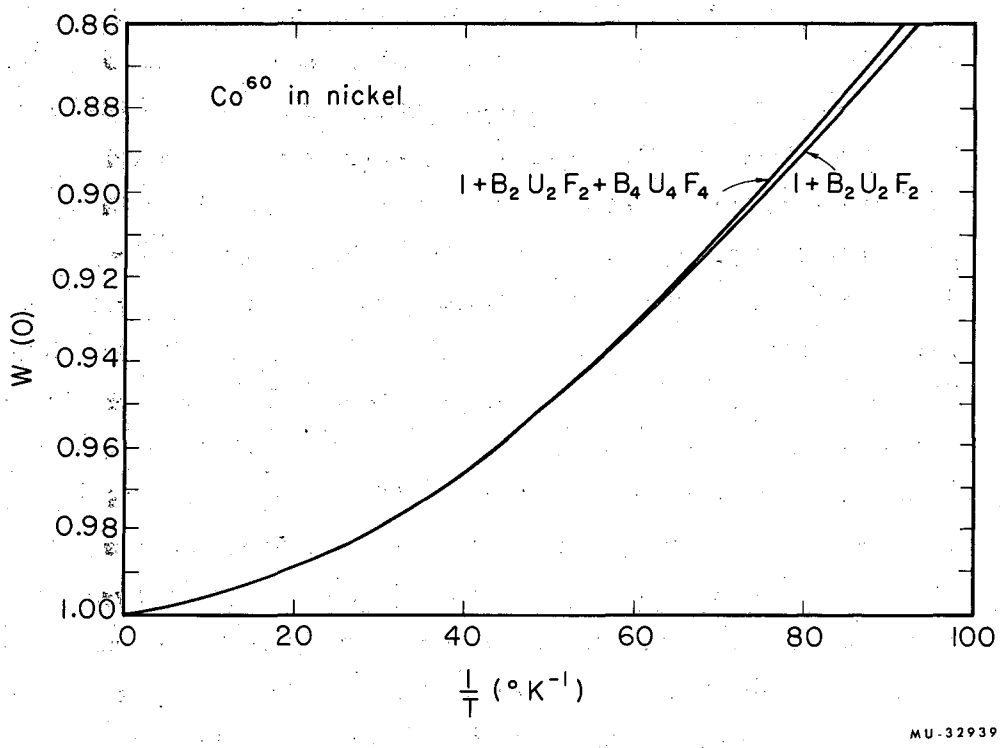

Fig. 14. Calculated temperature scale for Co^{60} in nickel; W(0) vs 1/T is plotted for $H_{int} = 120$ kG.

VI. RESULTS

A. Decay Scheme of Ag^{110m}

The isotope Ag^{110m} was polarized in iron and the angular distribution of γ radiation was measured. Ten γ rays were found to be anisotropic, although several were unresolved in the spectrum. The γ-ray spectrum of Ag^{110m} is shown in Fig. 15. The solid curve represents the normal high-temperature isotropic γ-ray intensity, while the dashed curve gives the intensities observed in the same geometry, parallel to the axis of polarization, but with the alloy cooled to near 0.01°K.

Figure 16 shows the magnitude of the anisotropy, W(0), as a function of photon energy. This curve shows that several γ rays that cannot be resolved by the counting equipment are also anisotropic.

A part of the most recently proposed decay scheme for Ag^{110m} is shown in Fig. 17. This decay scheme is the result of various electron and γ-ray spectroscopic measurements,[36] as well as a recent angular correlation experiment.[37] The data obtained by nuclear polarization of this isotope are analyzed below by using the level structure of this decay scheme. The interpretation of the results has led to unique spin assignments for three of the levels in Cd^{110}. The assignment of 5+ rather than 6+ to the 2925-keV level was made on the experimental observation that the 1383-keV γ ray is not an E2 transition. Spin 4+ for the 1542-keV level has previously been established. The observation that the 764-keV γ ray is an E2 transition, led directly to the assignment of 3+ to the 2161-keV level. The 2218-keV level was determined to be 4+ since the 707-keV γ ray was found not to be pure E2, which would be the case if the spin of this level were 3+. A detailed presentation of these experimental results for Ag^{110m} is given below.

The general scheme of analysis consisted of determination of an experimental value of $B_2U_2F_2$ for each γ ray. The k = 4 term was initially assumed to be negligible but was taken into account for the final evaluation. The temperature-dependent function, B_2, was

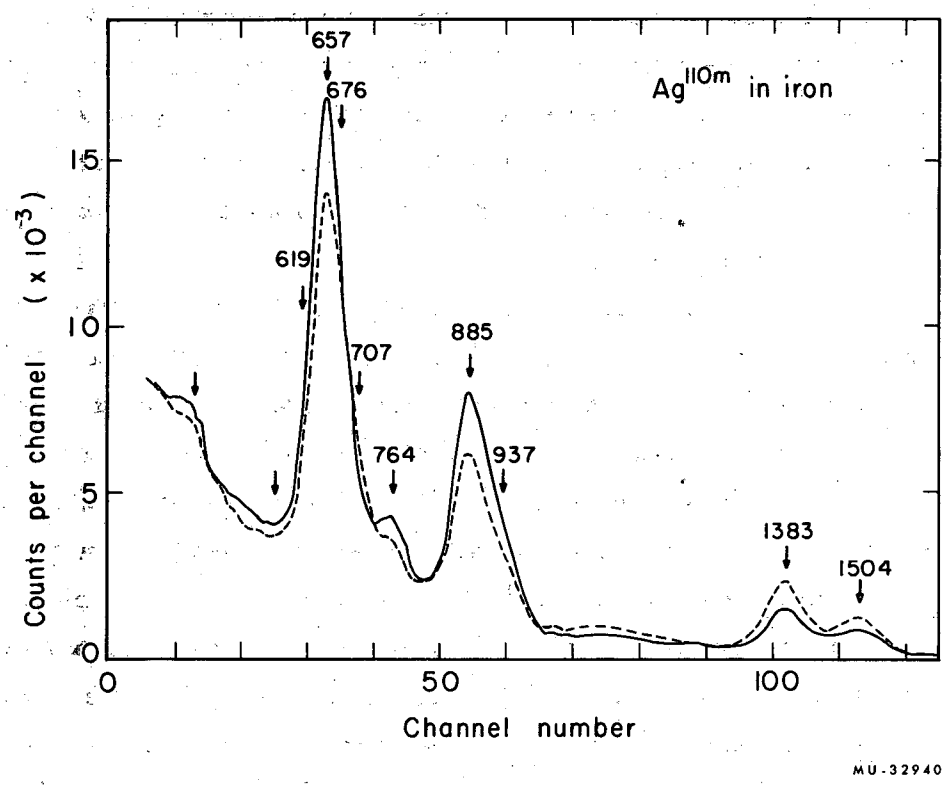

Fig. 15. Gamma-ray spectrum of Ag^{110m} obtained along polarizing axis with the iron alloy cooled to near 0.01°K (dashed curve) and about 1°K (solid curve).

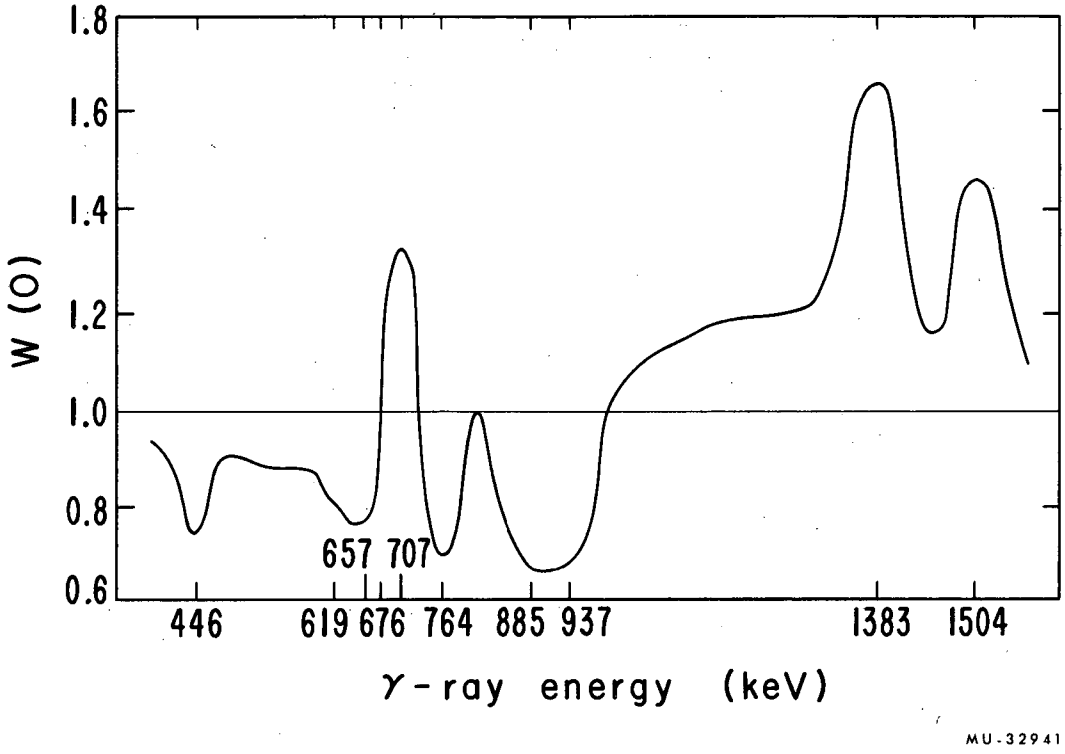

Fig. 16. Plot of W(0) vs photon energy for Ag^{110m} in iron. Several unresolved γ rays are clearly anisotropic.

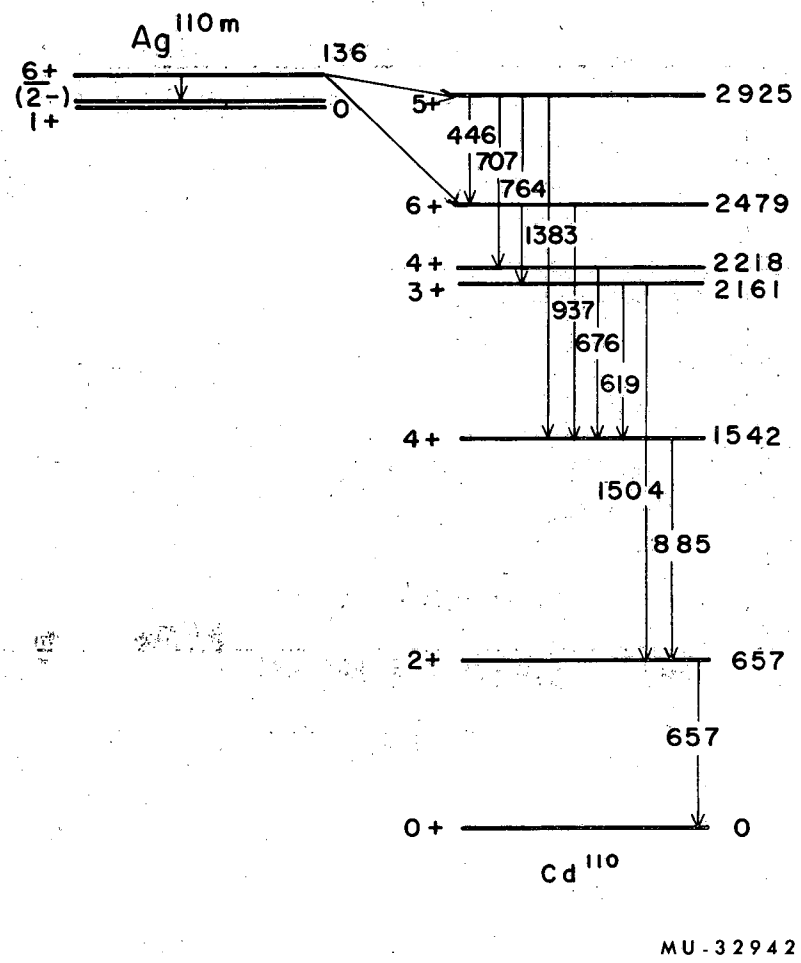

Fig. 17. Partial-decay scheme of Ag^{110m}, taken from reference 36.

then eliminated by calculating the ratio of $B_2U_2F_2$ for two γ rays. Then, if the U_2F_2 product for one γ ray was known, the U_2F_2 of the other could be determined. In general, U_2 is a slowly varying function of the parameters on which it depends and is usually very nearly unity. Little error was therefore introduced by estimating an initial value for U_2. Knowledge of U_2 for a particular γ ray allowed determination of F_2 for that γ ray. Various initial and final nuclear spins and multipolarities for the transition were used to fit these experimental F_2 coefficients.

The experimental F_2 values for two γ rays in cascade were then used to calculate the A_2 coefficient that would be determined by an angular-correlation experiment. These A_2 values were then compared to the available angular-correlation data. In general, the error in determination of A_2 is smaller for the nuclear-polarization experiment.

1. The 885-keV γ ray

The first requirement for this scheme of analysis was establishment of F_2 for any one of the γ rays in order to eliminate B_2. For this, it was assumed that the 885-keV γ ray was a pure E2 transition. The electron-conversion coefficient as well as the angular-correlation data establish this. The analysis was therefore based on $F_2(885) = -0.448$. The 885-keV γ ray was well resolved from all but the 937-keV γ ray, which has a low relative intensity, so that the accuracy of determining the experimental value of $B_2U_2F_2(885)$ was quite good. The result was $B_2U_2F_2(885) = -0.324 \pm 0.004$ at $1/T = 80$.

The experimental values of $B_2U_2F_2$ for the γ rays from Ag^{110m} are given in Table I. These data are all for $1/T = 80$. They were first corrected for counting geometry and for scattered background radiation under the γ-ray photopeaks. The background correction was not large except for γ rays of low energy and small intensity. The background may also be anisotropic and this fact was taken into account. The geometric correction was typically about 7%, but was accurately known.

Table I. Experimental values of $B_2U_2F_2$ for γ rays from Ag^{110m}.

Energy (keV)	Relative intensity	Experimental $B_2U_2F_2$ at 1/T=80
446	7	-0.26±0.13
619	<10	>-0.3
657	100	<-0.215±0.002
676	12	> 0
707	18	>+0.30
764	24	-0.30±0.02
885	75	-0.324±0.004
937	25	-0.31±0.01
1383	20	+0.680±0.007
1504	13	+0.480±0.006

2. The 657-keV γ ray

The experimental value of $B_2U_2F_2$ for the 657-keV region of the spectrum was -0.215±0.002. There is clear evidence in Fig. 16, however, that this part of the spectrum contains several γ rays of very similar energies. The 705-keV γ ray is not well resolved from the 657-keV peak, but it definitely has a large positive value for $B_2U_2F_2$ (705). The 619-keV and 676-keV γ rays are also not resolved but are easily shown to have $B_1U_2F_2 > B_2U_2F_2$ (657). Although these other γ rays are each relatively weak, together they cancel in part the anisotropy of the 657-keV γ ray and lower the magnitude of the experimental value of $B_2U_2F_2$ (657). If the above value of $B_2U_2F_2$ is used for $B_2U_2F_2$ (657), then,

$$\frac{B_2U_2F_2\ (657)}{B_2U_2F_2\ (885)} = \frac{U_2F_2\ (657)}{U_2F_2\ (885)} = +\ 0.66\pm0.02.$$

The total reorientation parameter U_2 for the 657-keV γ ray is the product of $U_2(\beta)$, $U_2(1383)$, and $U_2(885)$. The U_2 for the 885-keV γ ray is the product of $U_2(\beta)$ and $U_2(1383)$. Here, $U_2(885)$ refers to the reorientation produced <u>by</u> the 885-keV transition and is not to be confused with the U_2 parameter <u>for</u> the 885-keV γ ray. Thus, the ratio is

$$\frac{U_2F_2\ (657)}{U_2F_2\ (885)} \equiv \frac{U_2(\beta)\,U_2\,(1383)\,U_2\,(885)\ F_2\,(657)}{U_2(\beta)\,U_2\,(1383)\,F_2\,(885)} = +\,0.66\pm0.02.$$

The U_2 for the 4+ to 2+ pure E2 885-keV γ transition was calculated to be $U_2(885) = +\ 0.749$. This yielded an experimental $F_2(657) = -\ 0.40 \pm 0.01$. Use of the reorientation parameters for the other decay branch which feeds the 657-keV transition gave essentially the same result.

This F_2 value may be compared with the angular-correlation data for the 885-keV–657-keV γ-ray cascade for which $A_2 = 0.073\pm0.014$. To make this comparison, $F_2(885)$ was recalculated

for the 885-keV γ ray, since it was first in the correlation sequence. The F_2 determined by nuclear polarization is the same as the F_2 of angular correlation, if the γ ray is last in the cascade. The notation F_2^F and F_2^L will be used when necessary to distinguish between these related but different F_2 coefficients.[38,39] The A_2 of angular correlation is just the product $F_2^F F_2^L$ for the two γ rays in the cascade. If F_2^L is known for a particular γ ray, F_2^F for that γ ray is exactly determined. Thus, by this scheme, $F_2^F(885)$ was computed to be -0.171. This gave

$$F_2^L(657) = \frac{A_2(885\text{-}657)}{F_2^F(885)} = -\ 0.43 \pm 0.08.$$

The values of $F_2^L(657)$ for the two methods are clearly compatible. This agreement is due to the fact that both values suffer from the same error. Both the 619-keV and 676-keV γ rays are in rapid cascade with the 885-keV γ ray. Thus the angular correlation also includes the effect of these γ rays which are unresolved from the 657-keV peak. The 657-keV γ ray has been previously established to be the 2+ to 0+ transition in Ag^{110m}. This requires that $F_2(657) = -\ 0.598$. Use of this F_2 value and the experimental $B_2U_2F_2$ for the 657-keV region of the spectrum allows estimation of $B_2U_2F_2$ values for the 619-keV and 676-keV transitions.

3. <u>The 1383-keV γ ray</u>

The value of $F_2(1383)$ was determined by comparing $B_2U_2F_2$ for the 1383-keV γ ray to $B_2U_2F_2$ for the 885-keV γ ray. This experimental ratio is -2.10±0.05. Therefore,

$$\frac{F_2\ (1383)}{U_2(1383)F_2(885)} = -\ 2.10 \pm 0.05,$$

or $F_2(1383) = (-2.10 \pm 0.05)\ (0.94)\ (-0.448) = +\ 0.88 \pm 0.02$, where $U_2(1383) = +\ 0.94$ if the 1383-keV γ ray was temporarily assumed to be a pure M1 transition. The value of $F_2(1383)$ obtained in this way allowed δ, the E2/M1 mixing ratio of the 1383-keV transition,

to be determined approximately. Recalculation of $U_2(1383)$, using this mixing ratio, then yielded a better value for $F_2(1383)$ and for δ. Two such iterations yielded $F_2(1383) = +0.86 \pm 0.02$. This limited δ to $\delta(1383) = -0.033 \pm 0.015$ and established the 1383-keV γ ray to be 89±1% M1. The $U_2(1383)$ was thus determined to be $+0.911 \pm 0.006$. The only other possible interpretation was $\delta(1383) = -2$, which required an 80% E2 character for this γ ray. This value was eliminated by the conversion coefficient,[40] which indicates an M1 transition.

It is interesting to compare $F_2(1383)$ and $F_2(885)$ with the angular correlation result for this cascade. Use of $A_2 = -0.308 \pm 0.013$ for the 1383-keV—885-keV γ-ray cascade gave $F_2^L(1383) = +0.90 \pm 0.03$. This is consistent with the present experiment and is in agreement with the predominantly M1 character of the 1383-keV γ ray.

An independent determination of the $F_2(1383)$ was possible by comparison of the 657-keV γ ray and 1383-keV γ ray, since the 885-keV intermediate transition is pure E2. The experimental ratio of $B_2U_2F_2$ for these γ rays gave

$$\frac{F_2(1383)}{U_2(1383)\ U_2(885)\ F_2(657)} = -3.16 \pm 0.04.$$

With the $F_2(657) = +0.40 \pm 0.02$ determined above, this gave $\frac{F_2(1383)}{U_2(1383)} = +0.945 \pm 0.05$. The 1383-keV γ ray was initially assumed to be pure M1. Thus, initially the values are $U_2(1383) = 0.940$ and $F_2(1383) = +0.89 \pm 0.05$. Iteration gave $F_2(1383) = +0.87 \pm 0.05$ with $(-0.040 \leq \delta \leq -0.028)$. This is in quite good agreement with the above result, if one considers the reduced experimental value of $B_2U_2F_2(657)$ that was obtained. The 1383-keV γ ray must therefore have 89±1% M1 character.

A rough comparison with angular correlation was again possible. Use of the angular-correlation value, $A_2(1383\text{-}657) \approx -0.40$ with $F_2(657) = -0.40 \pm 0.02$, gave $F_2^L(1383) \approx +1.0$. The large implied error in A_2 may include the above more accurate result for $F_2(1383)$.

4. The 1504-keV γ ray

The experimental value of $B_2U_2F_2(1504)$ is $+0.480 \pm 0.006$. The ratio of this value to that for the 657-keV γ ray yielded

$$\frac{F_2(1504)}{U_2(1504)\cdot F_2(657)} = -2.47 \pm 0.05,$$

which finally gave $F_2(1504) = +0.73 \pm 0.06$ with $\delta(1504) = -0.05 \pm 0.02$. This implied a > 99% M1 character for the 1504-keV γ ray. The conversion coefficient again rules out the possibility of a large E2 admixture.

The experimental A_2 for the 1504-keV–657-keV cascade was given as $-0.47 \leq A_2 \leq -0.27$. The above experimental value of $F_2(657)$ gave values of $F_2^L(1504)$ from +0.35 with 6% M1 to +0.98 with 83% M1. This result is not actually in agreement with the polarization value because of the double-valued property of the mixing ratio.

After assumption of the theoretical value for $F_2(657)$, the value of $F_2(1504)$ obtained was between +0.80 and +1.08, which probably better represents the angular—correlation result. This range of $F_2(1504)$ allowed 93 to 69% M1 character for the 1504-keV transition. The present determination of $F_2(1504)$ indicates the lowest value $F_2(1504)$ of the above range having the highest M1 character is probably most accurate.

The value of $F_2(1504)$ was also determined from the ratio of the anisotropies of the 1504-keV and 764-keV γ rays. The 764-keV transition is E2 according to the decay scheme of Ag^{110m}. By making this assumption initially, it was possible to show that the 1504-keV γ ray has $F_2(1504) = +0.79 \pm 0.06$ with $\delta(1504) = -0.25 \pm 0.05$ and $93 \pm 2\%$ M1 character. This result is in good accord with the above determination of $F_2(1504)$, and thus it confirms the E2/M1 mixing ratio for the 1504-keV γ ray and also verifies the E2 character of the 764-keV γ ray. The spin of the 2161 level was thus confirmed to be I = 3+.[36]

The angular-correlation measurement for the 764-keV—1504-keV γ ray cascade gave $+0.53 \leq F_2^L(1504) \leq +1.18$ for $-0.27 \leq A_2 \leq -0.12$. This range includes the best nuclear-polarization value of $F_2(1504) = +0.73 \pm 0.06$.

5. The 937-keV γ ray

The ratio of the 937-keV and the 885-keV γ-ray anistropies gave $F_2(937) = -0.388 \pm 0.015$, which agrees with the value -0.402 for a pure E2 transition.

The 937-keV—885-keV γ-ray cascade gave $+0.123 \leq A_2 \leq +0.177$. This gave $-0.395 \leq F_2^F(937) \leq -0.275$, which does not include the pure E2 value $F_2^F(937) = -0.228$.

6. The 707-keV γ ray

This γ ray and the 1383-keV γ ray have a common U_2. So, the ratio is simply

$$\frac{F_2(707)}{F_2(1383)} > +0.44.$$

But, since $F_2(1383) = +0.86 \pm 0.02$, the value of the other coefficient is $F_2(707) > +0.38$. If the 707-keV transition is $5+ \rightarrow 3+$, $F_2(707)$ would be -0.420 for this pure E2 decay. The anisotropy is clearly positive in Fig. 16, and thus the conclusion is that the 2218-keV level is not $I = 3+$. The value $I = 5+$ was also ruled out by the lack of a strong β branch to this state. Only the assumption of $I = 4+$ for this level makes $F_2 > +0.38$ possible. The uncertainty in $F_2(707)$ prevents a clear analysis of the mixing ratio for this γ ray. It was indicated only to be from 1 to 96% M1. The spin of this state was determined for the first time.

7. The 446-keV γ ray

The large background under this peak and its low intensity make the anisotropy determination quite inaccurate. The best value was $B_2U_2F_2(446) = -0.26 \pm 0.13$. This γ ray and the 1383-keV γ ray

have a common U_2 so that

$$\frac{F_2(446)}{F_2(1383)} = -0.38 \pm 0.19.$$

This gave $F_2(446) = -0.33 \pm 0.17$. For a 5+ to 6+ transition, this value of $F_2(446)$ gave an E2/M1 mixing of 17 to 87% M1 character.

8. The 619-keV and 676-keV γ rays

These two relatively weak transitions are not resolved from the intense 657-keV γ-ray peak. Careful analysis of curves such as Fig. 16 in which one uses the relative intensities of the three γ rays as a guide allowed only a crude estimate of the anisotropies. The sign of $B_2U_2F_2$ for the 619-keV γ ray was established to be negative. The 676-keV γ ray is more uncertain but was necessarily positive.

These transitions are supposed to be 3+ to 4+ and 4+ to 4+, respectively, so that M1-E2 mixing is possible. The conversion coefficients give definite indication of strong M1 character. The present data allow any E2/M1 ratio for either γ ray, however.

9. Summary

The decay scheme of Ag^{110m} given in Fig. 17 has been shown to be consistent with the nuclear-polarization data. The possibility of spin 4+ for the 2161 level was eliminated and the spin of the 2218-keV level was found to be I = 4+. The 657-keV, 707-keV, 764-keV, 885-keV, and 937-keV γ rays were found to be pure E2 transitions. The 1383-keV and 1504-keV γ rays were found to be mixed M1-E2 with 89 ± 1% M1 and > 99% M1, respectively. Three other γ rays were found to anisotropic, but mixing ratios could not be accurately assigned.

B. Magnitude of the Hyperfine Interaction

The magnitude of the hyperfine splitting for Ag^{110m} in iron and nickel was determined from the experimental value of B_2. At a particular temperature, the value of B_2 is dependent upon the relative population of the $2I + 1$ magnetic hyperfine levels. The population of a given level depends upon the energy differences between levels and thus upon the product μH according to Eq. (1), where H is the effective internal magnetic field at the silver nucleus and μ is the nuclear-magnetic moment of Ag^{110m}. Since neither the sign nor magnitude of either μ or H is known, only the product can be determined by the present experiment.

To obtain B_2 experimentally, the value of $B_2U_2F_2$ for the 657-keV, 884-keV, and 1504-keV γ rays were determined as a function of temperature. The $B_4U_4F_4$ term was initially assumed to be negligible, but was taken into account in determining the final value of $B_2U_2F_2$ for each γ ray. The highly anisotropic 1383-keV γ ray was not included in the analysis because of the interference of the unresolved 1333-keV γ ray from the Co^{60} thermometer. The results are entirely satisfactory without use of this γ ray, however.

The U_2F_2 product, which was determined for each of these γ rays by analysis of $B_2U_2F_2$ ratios in Sec. VI-A, was used to determine an experimental B_2 for each temperature point. These experimental B_2 versus experimental temperature points were then compared with calculated B_2 versus temperature curves that were obtained by using various values of μH and Eq. (4). The experimental μH value was then obtained by best fit of the theoretical curves.

Figure 18 shows the experimental values of B_2 and several theoretical curves for Ag^{110m} in iron. The experimental B_2 values were obtained by averaging the values determined for each of the three γ rays. The best μH value was thus found to be $|\mu H| = (9.0 \pm 0.5) \times 10^5$ nm gauss. Figures 19, 20 and 21 show, respectively, the experimental values of $B_2U_2F_2$ as a function of

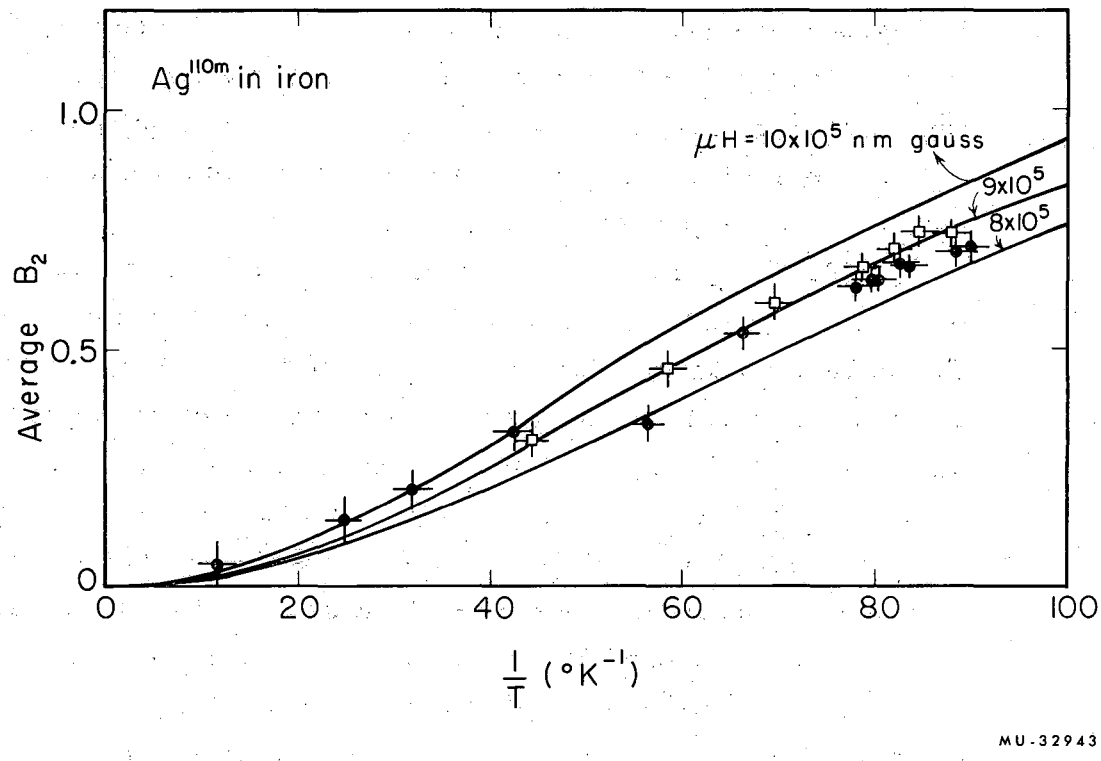

Fig. 18. Average value of B_2 obtained by analysis of three γ rays from Ag^{110m} in iron plotted as a function of 1/T. The curves were calculated by using the values of μH shown.

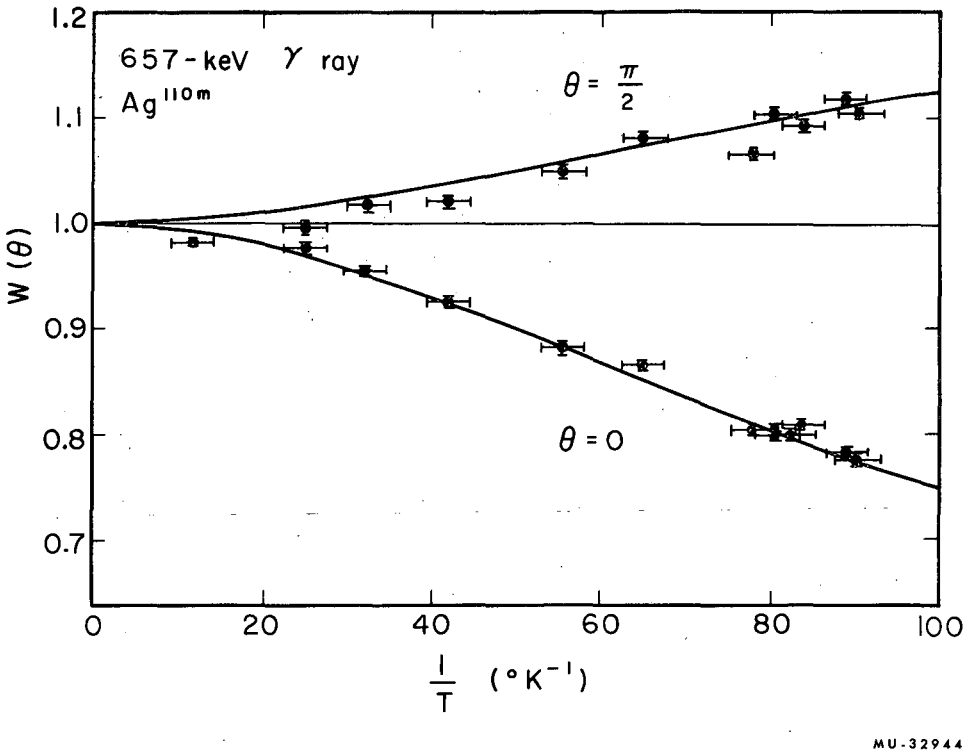

Fig. 19. Experimental $W(\theta)$ for 657-keV γ ray from Ag^{110m} in iron vs $1/T$. Solid curves are for $\mu H = 9 \times 10^5$ nm gauss.

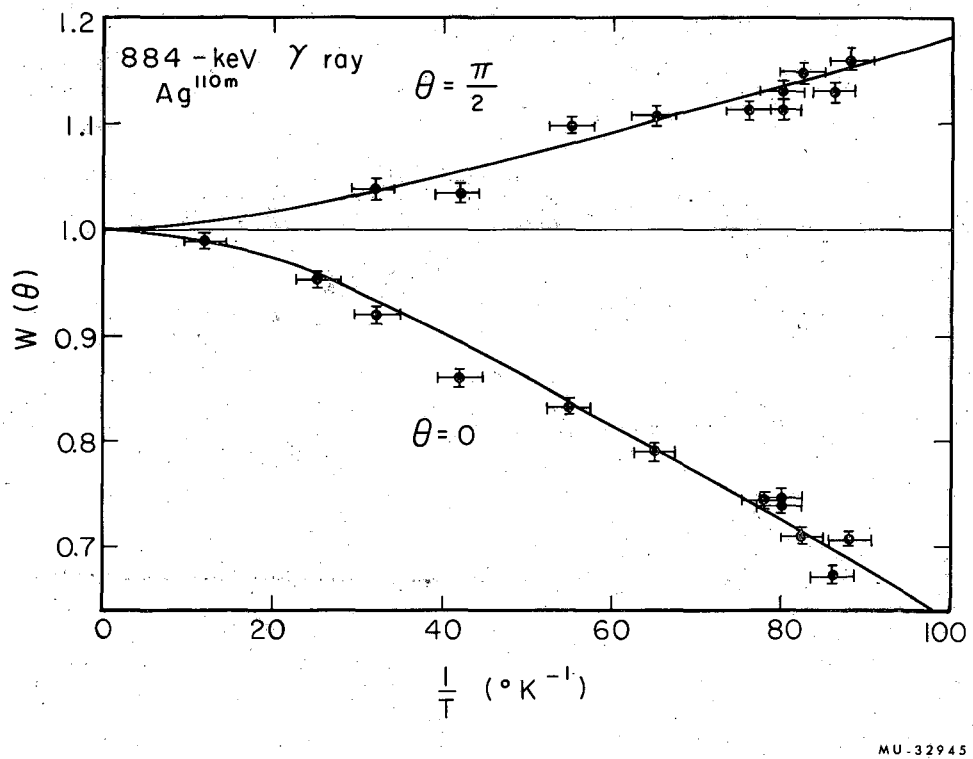

Fig. 20. Experimental $W(\theta)$ for 885-keV γ ray from Ag^{110m} in iron vs 1/T. Solid curves are for $\mu H = 9 \times 10^5$ nm gauss.

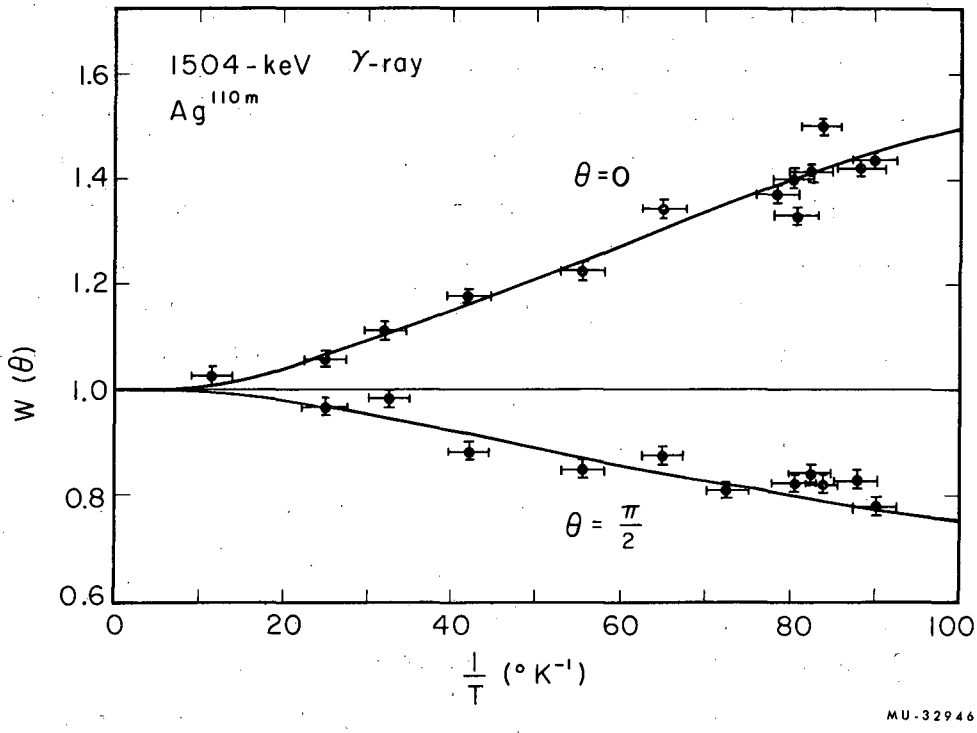

Fig. 21. Experimental $W(\theta)$ for the 1504-keV γ ray from Ag^{110m} in iron vs $1/T$. Solid curves are for $\mu H = 9 \times 10^5$ nm gauss.

temperature for the 657-keV, 885-keV, and 1504-keV γ rays from Ag^{110m} in iron. The solid curves are for the μH value given above. Data for the 1383-keV γ ray are shown in Fig. 22. These were obtained with an alloy which did not contain a Co^{60} thermometer. The temperature was determined from W(0) for the 1504-keV γ ray and Fig. 21.

Because of the low solubility of silver in iron, the magnitude of μH was also determined for a more dilute alloy. This would determine whether the silver was completely dissolved or only partially dissolved in the iron. The experimental value of μH obtained was essentially identical to that given above within the error of the measurement. As an additional check on the size of μH for the iron alloy, the value of $B_4U_4F_4$ was determined by comparison of the axial and equatorial anisotropies. This yielded an essentially independent value for μH.

Two special cases of Eq. (3) are

$$W(0) = 1 + B_2U_2F_2 + B_4U_4F_4$$

and

$$W(\tfrac{\pi}{2}) = 1 - 1/2\, B_2U_2F_2 + 3/8\, B_4U_4F_4 \,.$$

From these the k = 4 term is obtained as

$$B_4U_4F_4 = 4/7\, [\, W(0) + 2\, W(\pi/2)] \,,$$

where W(0) and $W(\frac{\pi}{2})$ are the normalized axial and equatorial counting rates, respectively. An experimental U_4 and F_4 was derived from U_2 and F_2 for the 885-keV γ ray. Also, B_4 was calculated as a function of temperature for various values of μH by use of Eq. (5). The theoretical $B_4U_4F_4$ was then compared to the experimental values. Figure 23 shows the theoretical curves and the experimental points for the 884-keV γ ray. The μH product for Ag^{110m} in iron must be at least $(9 \pm 1) \times 10^5$ nm gauss, which includes the range of the analysis above.

A similar analysis of the temperature dependence of the anisotropy of the 657-keV, 884-keV, and 1504-keV γ rays from

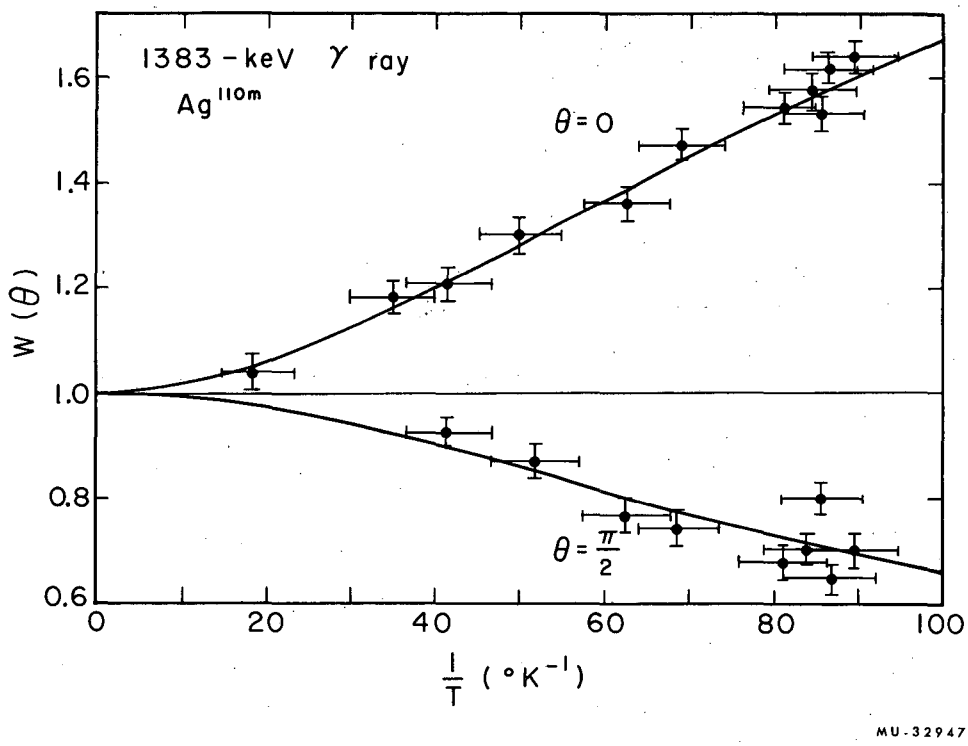

Fig. 22. Experimental $W(\theta)$ for 1383-keV γ ray from Ag^{110m} in iron vs $1/T$. Solid curves are for $\mu H = 9 \times 10^5$ nm gauss.

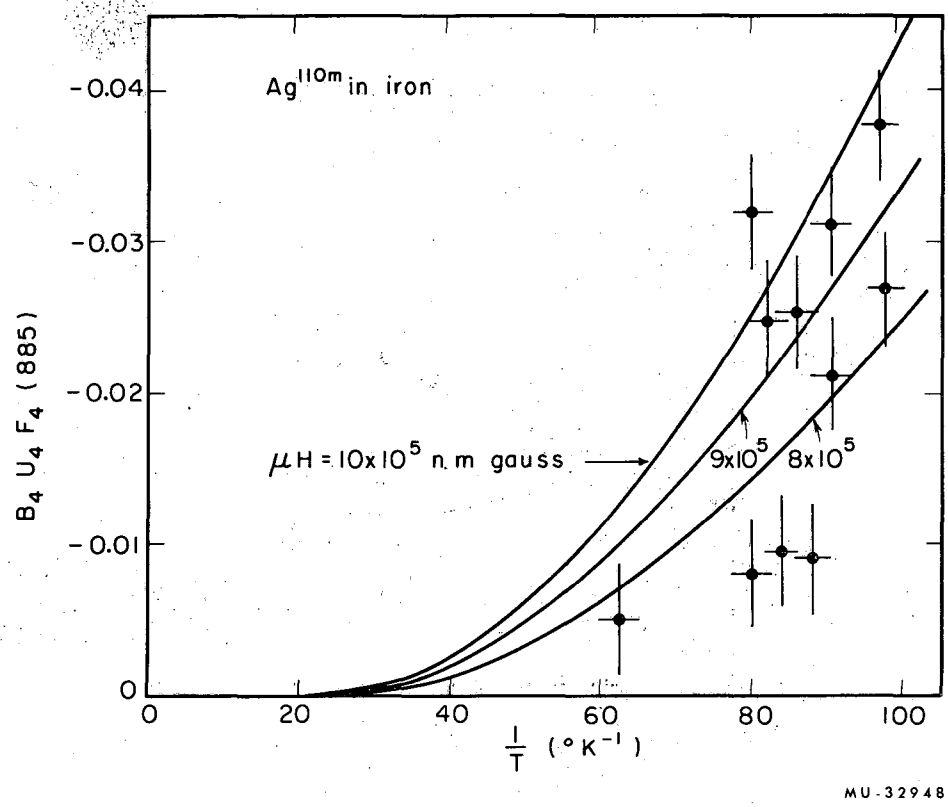

Fig. 23. Experimental $B_4U_4F_4$ (885)for Ag^{110m} in iron vs 1/T. Curves calculated for three values of μH are shown.

Ag^{110m} polarized in nickel yielded the μH value for the nickel alloy. The $B_2U_2F_2$ values for the three γ rays gave an average value of $|\mu H| = (3.0 \pm 0.3) \times 10^5$ nm gauss. The average B_2 values obtained are shown in Fig. 24. The $B_4U_4F_4$ term was negligible even at the lowest temperature and was therefore not used in the analysis.

C. Sign of the Hyperfine Interaction

First one needs to consider the angular distribution of electrons from the allowed β decay of polarized Ag^{110m}. The angular-distribution function, $W(\theta)$, was given in Eq. (6). The magnitude of the parameter B_1 depends upon the population of each of the hyperfine levels, while the sign of B_1 depends upon the ordering of the levels. The order of the magnetic states is determined by the sign of the product μH so that the experimental determination of the sign of B_1 gives directly the sign of μH.

This dependence on μH can be shown by expanding the function B_1 in powers of the parameter β of Eq. (2). When only the large first-order terms are taken, the angular-distribution function becomes

$$W(\theta) = 1 + 1/3 \frac{I+1}{I} \frac{\mu H}{kT} \left(\frac{v}{c}\right) A_- \cos\theta . \tag{9}$$

Here it is clearly seen that the sign of μH is determined directly from the asymmetry of the β emission provided the sign of A_- is known.

For Ag^{110m} polarized in iron, the expansion of B_1 gives

$$|B_1| = 1/3 \frac{I+1}{I} \left(\frac{|\mu H|}{kT}\right) = 1.03$$

for $1/T = 80$ and $\mu H = 9.0 \times 10^5$ nm gauss. An exact calculation using the full expression for B_1 gave $B_1 = 1.189$. The error incurred in using the approximate expression above is not significant for the present discussion but would need to be taken into account for a quantitative interpretation of the β asymmetry.

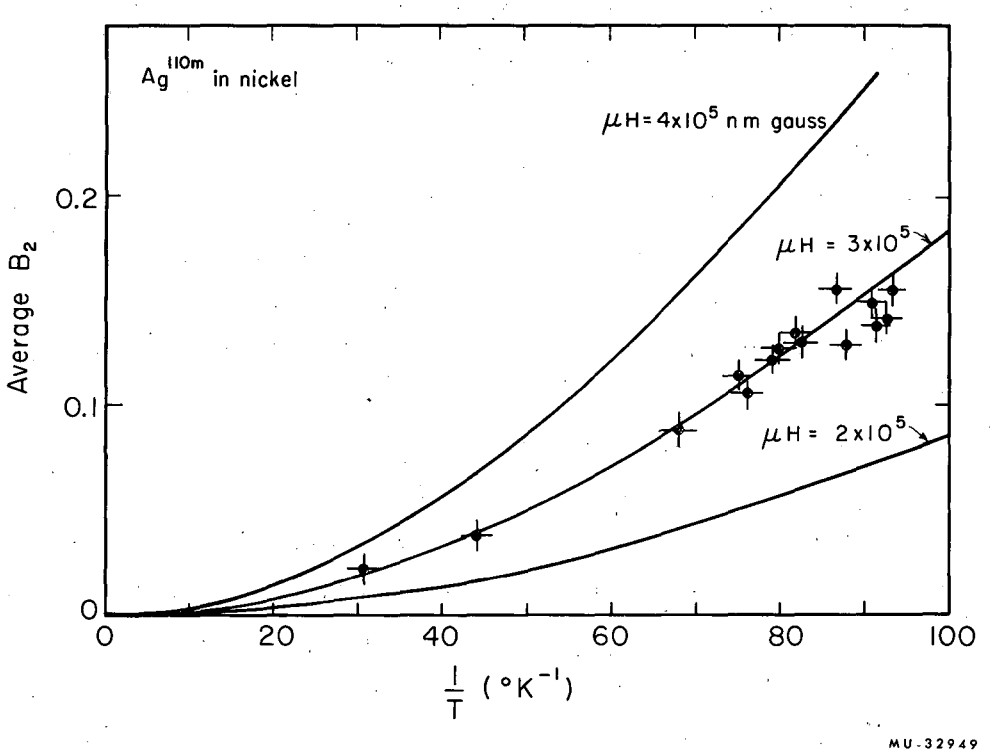

Fig. 24. Average value of B_2 obtained by analysis of three γ rays from Ag^{110m} in nickel plotted as a function of 1/T. The curves were calculated by using the values of μH shown.

The more intense 87-keV β branch from Ag^{110m} has too low an energy to be detected by the β counting system. Even at maximum gain the lowest electron energy detectible was about 150 keV. This was determined by counting the conversion electrons from a thin source of Hg^{203}. The electron spectrum obtained is shown in Fig. 25. The resolution is about 10% for these electron energies. The 530-keV electron branch was easily detectible however, because of its higher energy. Also, these electrons are better able to get out of the metal with less scattering. The counting rate is therefore higher and the asymmetry is less attenuated by scattering. The maximum asymmetry is also larger since the term v/c in Eq. (9) may become large. This factor is positive and for the end point of the 530-keV β branch it is equal to 0.87. For 400-keV electrons the value drops to 0.70, and for 87-keV electrons the value is 0.27.

The angular factor in Eq. (9) is determined by defining θ as the angle between the positive direction of the polarizing field and the β counter. When counting is done along the polarizing field direction, θ is 0 by definition; and thus $\cos\theta = +1$ is required in Eq. 9.

The remaining factor, A_-, contains all the nuclear parameters that characterize the β decay. There is no angular-momentum change during the 530-keV decay branch, so the radiation may be a mixture of Fermi and Gamow-Teller components. In this case, the existence of an interference term as given by Eq. (7) is possible and must be considered.

Measurement of the β-γ circular-polarization correlation indicated that the 530-keV β branch is essentially pure Gamow-Teller radiation.[41] The result given was

$$\frac{C_V M_F}{C_A M_{GT}} = 0.05 \pm 0.04$$

for

$$A_{\beta-\gamma} = +0.09 \pm 0.03.$$

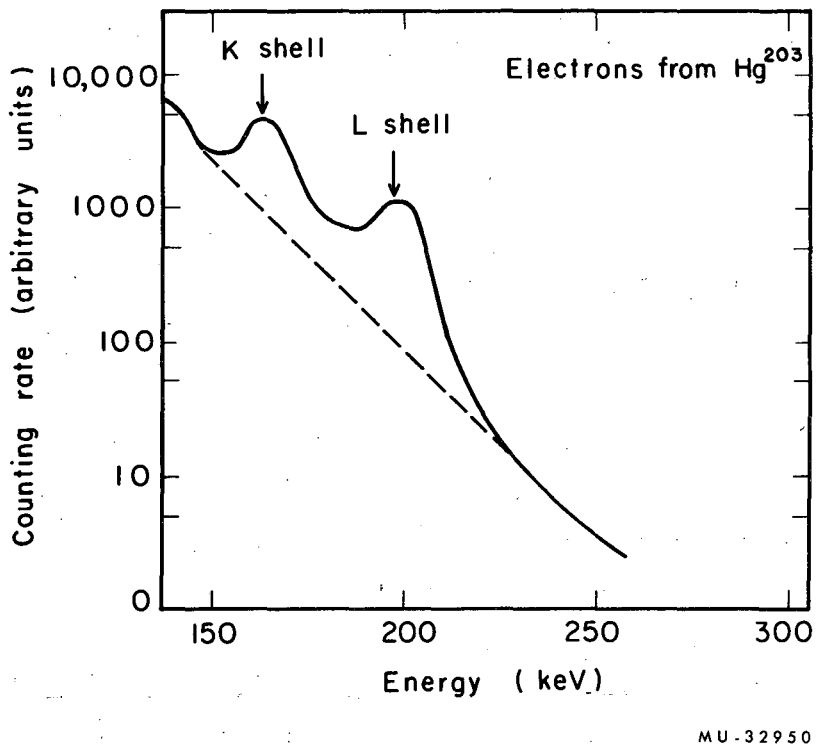

Fig. 25. Electron spectrum of Hg^{203} obtained with germanium counter at 4.2°K. Resolution of conversion lines is about 10%.

Therefore the interference term cannot be very large, since very little Fermi component is observed. Thus, the effect of interference on the asymmetry parameter A_- is small and can be neglected for the present discussion.

The assumption that the 530-keV β branch is pure Gamow-Teller radiation allows A_- to be evaluated by Eq. (8). Thus, A_- is

$$A_- = - \frac{1}{I + 1} = - \frac{1}{7} .$$

The addition of a small amplitude of Fermi radiation cannot change the sign of A_-, and so the sign of μH may be determined unambiguously. The negative value of A_- changes the sign of the asymmetry term in Eq. (9) so that this equation becomes

$$W(\theta) = 1 - a \mu H \cos \theta ,$$

where $a = 0.11 \times 10^{-6}$ at $1/T = 80$ for 400-keV electrons. The magnitude of μH allowed prediction of the asymmetry to be expected. For the conditions given above, the counting rate should change by about 10% when the material is cooled.

Beta counting was done with the alloys at near 0.01°K and at about 1°K with the polarizing field directed both toward and away from the counter; i.e., counting was done at $\theta = 0$ and $\theta = \pi$. The sign of the asymmetry should thus change according to the sign of $\cos \theta$.

There are four possible combinations of μ and H, since the sign of neither is known and either may be positive or negative. Here a negative internal field means that it is opposed to the polarizing field, while a negative moment means that the nuclear spin is antiparallel to the moment.

The possible combinations of internal field, magnetic moment, and counting angle are shown in Fig. 26. Two examples of the directional arrangement are shown in the diagrams for cases C and D. Case C represents the arrangement of vectors for $\theta = 0$ and negative μH product, while case D is for $\theta = \pi$. In practice, the counter was not moved physically to $\theta = \pi$ but rather the polarizing field was reversed as shown.

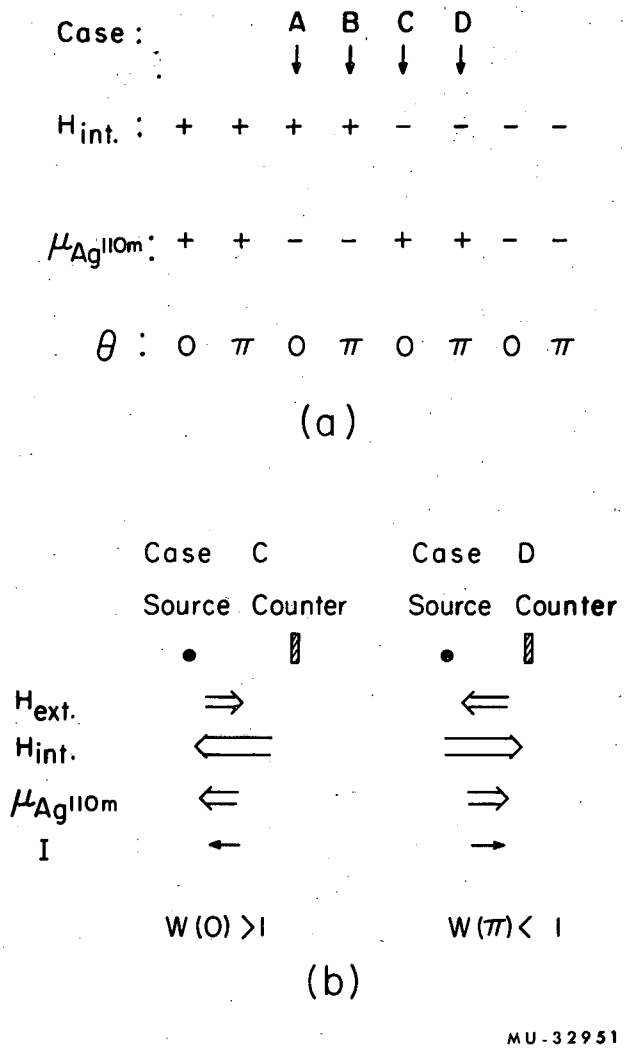

Fig. 26. Possible combinations of internal field and magnetic moment of Ag^{110m}. For Case C $W(0) > 1$ is predicted by Eq. 9. For Case D, $W(\pi) < 1$ is predicted.

With the results of the above analysis, it was then possible to interpret the experimental β asymmetry of Ag^{110m} polarized in iron and nickel. The alloys used for the β measurements did not contain a Co^{60} thermometer since the β's emitted by the thermometer would invalidate the measurement for Ag^{110m}. The temperature of the alloy was therefore monitored by measurement of the γ-ray anisotropy of the silver.

The small solid angle subtended by the sensitive part of the β counter required rather long counting periods. The initial temperature of the alloy was measured by a short γ-ray count within 3 minutes after the end of demagnetization. The long β count was then taken and then another short γ-ray count. The average temperature during the counting period could thus be obtained rather well from the γ-ray anisotropies. Twenty minutes was required for a typical β count. The temperature usually varied less than 2 millidegrees during the counting period, however.

As an experimental check on the counting equipment and on the interpretation of the sign of μH, an alloy of Co^{60} in iron was cooled to near 0.01°K and the electrons emitted from it were counted. For Co^{60} the sign and magnitude of both μ and H are known and so $W(\theta)$ may be calculated exactly, since the β- decay is a 5+ to 4+ pure Gamow-Teller transition. All uncertainty is therefore removed from the sign of the β asymmetry. Figure 27 shows the β spectrum obtained from Co^{60} in iron at an average temperature of about $1/T = 80$. This spectrum was obtained along the polarizing field at $\theta = 0$. Figure 28 shows the spectrum obtained from the same alloy when the polarizing field was reversed in a subsequent demagnetization. No energy scale was determined for this spectrum; however, the end-point electron energy is 312 keV.

For Co^{60} in iron, the result was $W(0) > 1$ and $W(\pi) < 1$, as would be predicted for a positive magnetic moment and negative internal field. This showed the asymmetry interpretation scheme to be correct and allowed the Ag^{110m} asymmetry to be correctly analyzed by comparison to this known case.

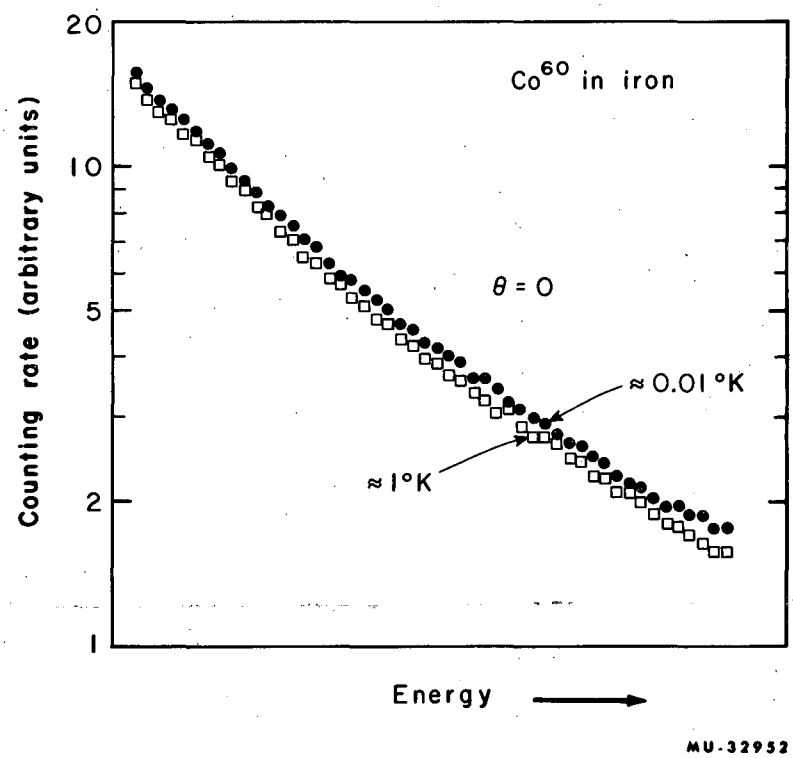

Fig. 27. Electron spectrum of Co^{60} in iron at $\theta = 0$; $W(0) > 1$ is correctly predicted.

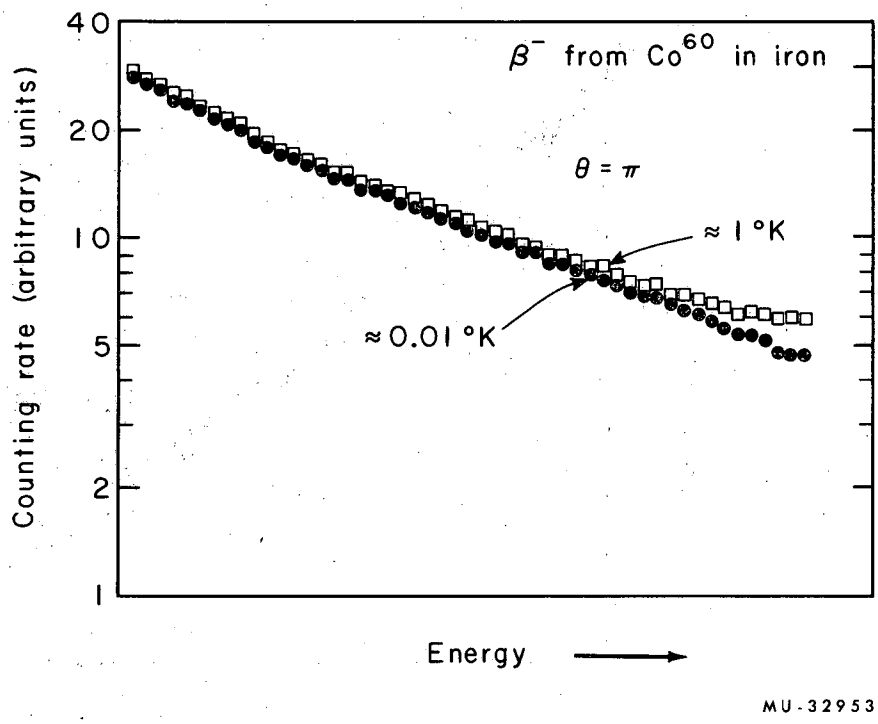

Fig. 28. Electron spectrum of Co^{60} in iron at $\theta = \pi$; $W(\pi) < 1$ is clearly shown.

A β spectrum obtained from Ag^{110m} polarized in iron at $1/T = 80$ is shown in Fig. 29. For $\theta = 0$ the result was $W(0) > 1$. This fact alone established that the product μH for Ag^{110m} in iron is negative according to Eq. (9). The ultimate proof was obtained by reversing the polarizing field so that the counter was then at $\theta = \pi$. Figure 30 shows the β spectrum thus obtained. Here it is clear that $W(\pi) < 1$, confirming that μH for Ag^{110m} in iron is negative. This experiment was repeated several times with different alloys and the results were consistent.

The experiment was then repeated with an alloy of Ag^{110m} in nickel. A spectrum for $\theta = 0$ is shown in Fig. 31 and for $\theta = \mu$ in Fig. 32. As was the case for the iron alloy, $W(0) > 1$ and $W(\pi) < 1$, which established that the μH product is negative in nickel also.

The immediate conclusion was that regardless of the sign of the magnetic moment of Ag^{110m}, the internal magnetic field at the silver nucleus has the same sign in both iron and nickel. Also, the knowledge that μH is negative limits the possible arrangements shown in Fig. 26 to either cases A and B or to C and D.

It was also necessary to establish what influence the experimental conditions had on the counter itself. Little is known about the characteristics of these germanium surface-barrier counters. It was established empirically that the gain of the counter is very sensitive to temperature changes. Spectra taken with the counter at 4.2°K and at 1°K showed that the gain increased markedly as the temperature was lowered. For this reason, care was always taken to ensure that the counter remained at the same temperature for the cold counting period, as was done for the count taken for normalization at the isotropic counting rate. The warm exchange gas was introduced to the cryostat very slowly to allow the gas to attain equilibrium with the helium bath before coming in contact with the counter. Later it was found convenient to eliminate the addition of exchange gas entirely by warming the salt assembly mechanically. This was done by rapping on the upper end of the pumping tube to cause vibrational heating. The warming was rapid and was monitored with the susceptibility bridge.

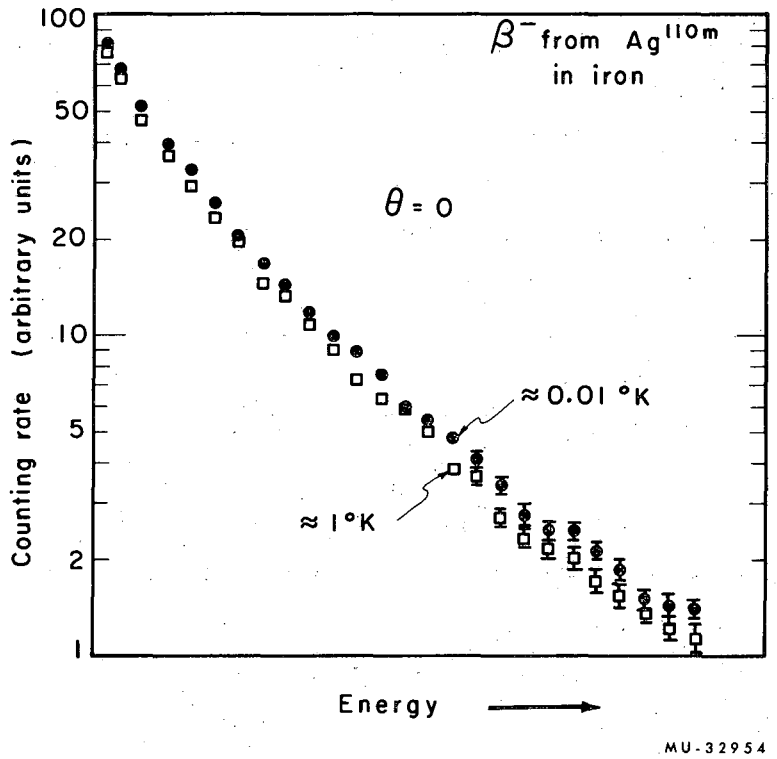

Fig. 29. Electron spectrum of Ag^{110m} in iron at $\theta = 0$; W(0) is shown to be greater than 1.

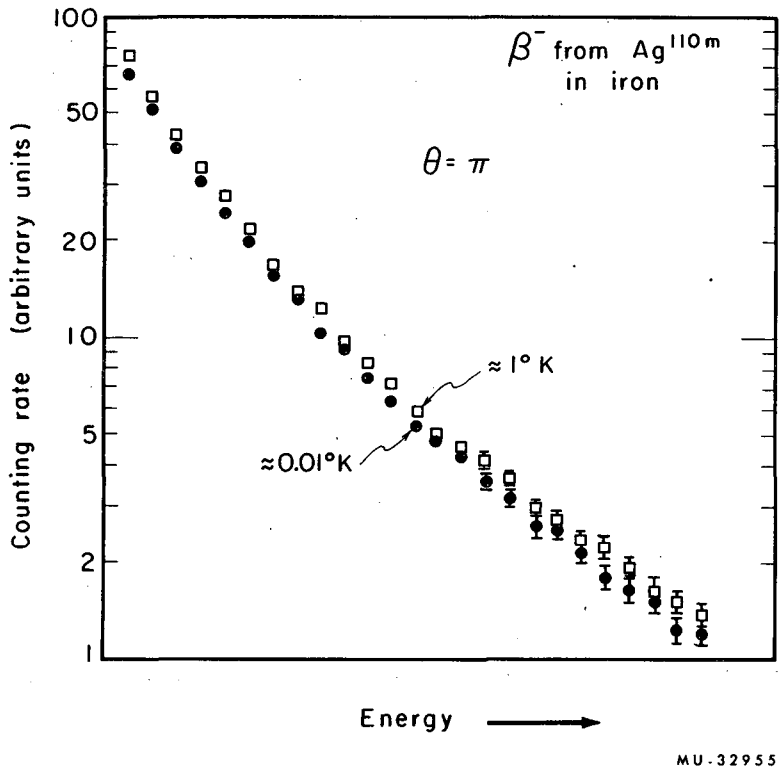

Fig. 30. Electron spectrum of Ag^{110m} in iron at $\theta = \pi$. Note that $W(\pi) < 1$.

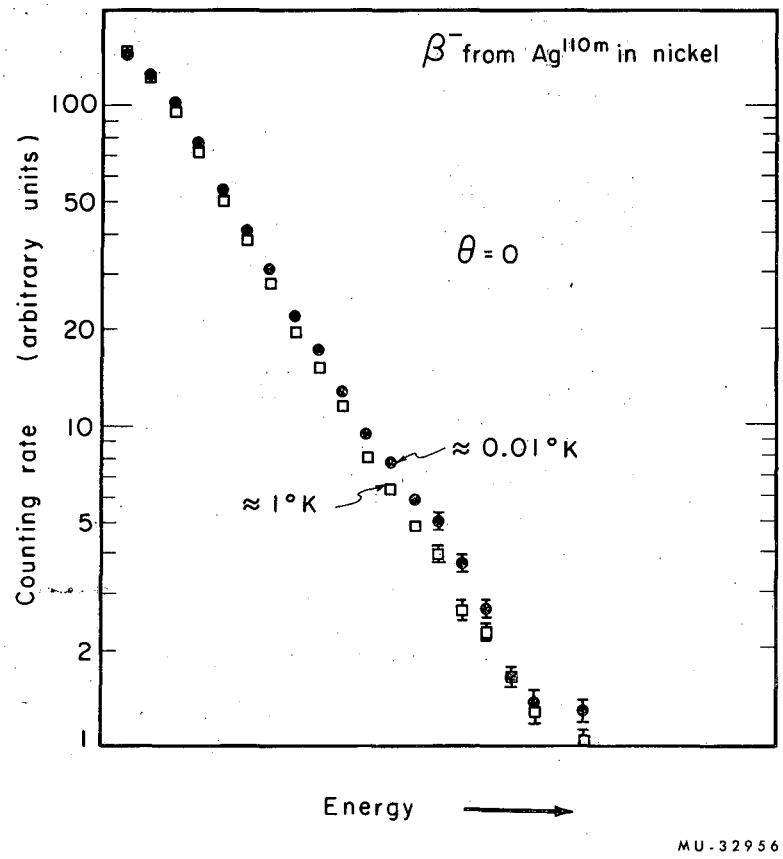

Fig. 31. Electron spectrum of Ag^{110m} in nickel at $\theta = 0$. Note that W(0) is greater than 1.

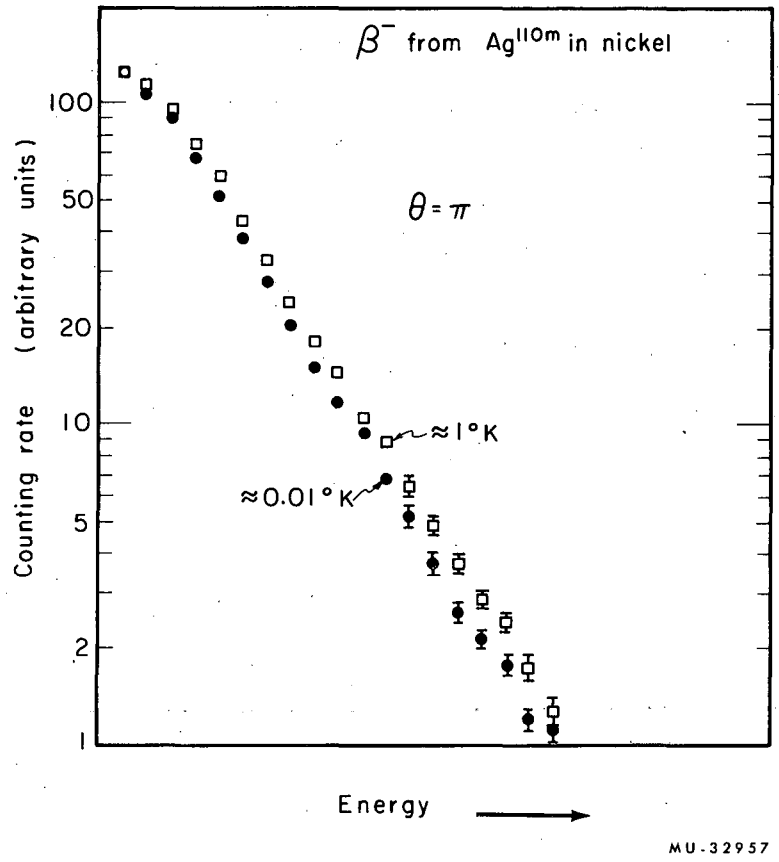

Fig. 32. Electron spectrum of Ag^{110m} in nickel at $\theta = \pi$. Note that $W(\pi) < 1$.

The effect of the magnetic field on the counter was not critical, since the counter was in the same steady field for both the cold count and the normalizing count. No difference could be detected by comparing spectra obtained at 1°K with the polarizing field in the normal and reversed directions. There seems to be no reason therefore to question the asymmetry measurement on grounds of anomalous counter behavior.

D. Polarization of Ag^{104}

The 27-min and 69-min isomers of Ag^{104} were prepared by a 2-hr bombardment of Pd^{104} with 18-MeV protons from the Berkeley 88-inch cyclotron. The nuclear reaction was $Pd^{104}(p,n)Ag^{104}$. An iron alloy was made which contained 5% palladium and the Ag^{104} activities. The polarization experiment was assembled in the manner previously described and the first demagnetization performed about 3 hr after bombardment.

The decay scheme of Ag^{104} is shown in Fig. 33.[42] Both the 785-keV and 920-keV γ rays were found to be anisotropic when the iron was polarized and cooled to about 0.017°K. The 555-keV region of the spectrum contained both the 555-keV γ ray and the 511-keV positron-annihilation radiation. This composite peak was found to be essentially isotropic in every case. This lack of anisotropy is probably due to a significant positron-annihilation background.

Two γ-ray spectra are shown in Fig. 34. The solid curves are the isotropic counting intensities parallel and perpendicular to the polarization axis. The dashed curves are the counting intensities in the same geometry but with the alloy polarized at about 0.017°K.

The temperature of the alloy was determined by measuring the magnetic temperature of the salt and by using the experimental correlations shown in Fig. 10. The lowest temperature at which counting was performed was about 0.017°K, where the correlation is quite reliable owing to the steep rise of the correlation curves.

The temperature dependence of the function W(0)-1 for the 920-keV γ ray is shown in Fig. 35. Two sets of values for the

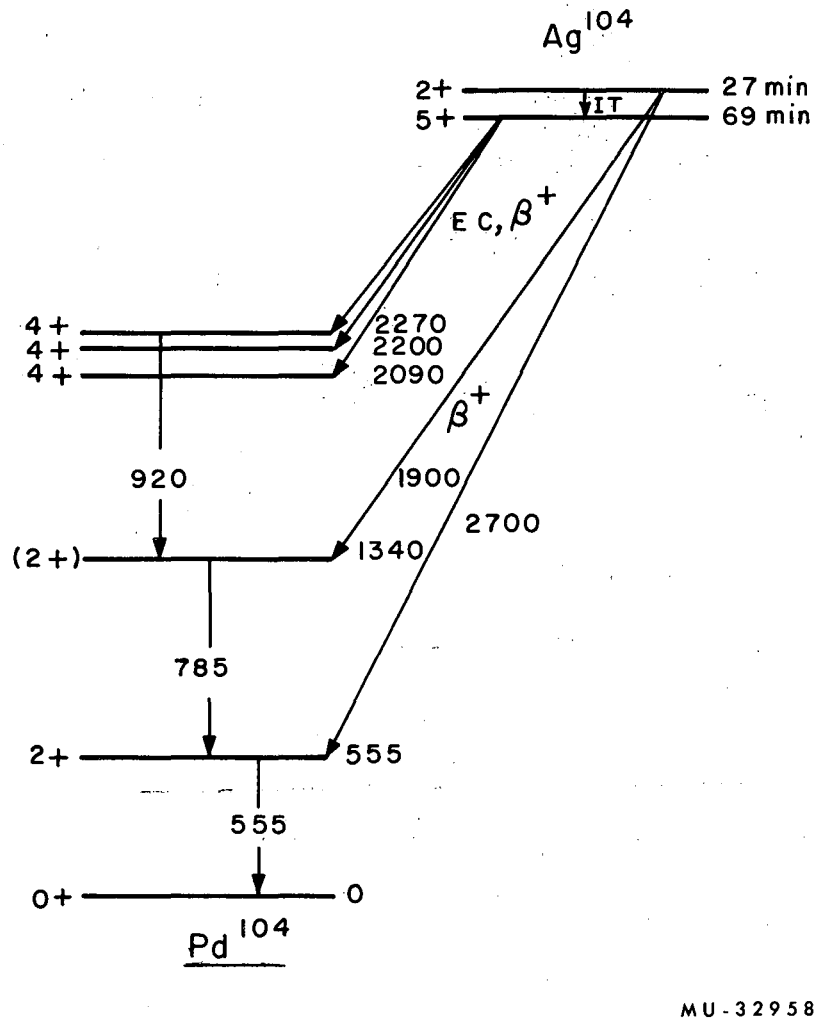

Fig. 33. Partial decay scheme for Ag^{104} following reference 42.

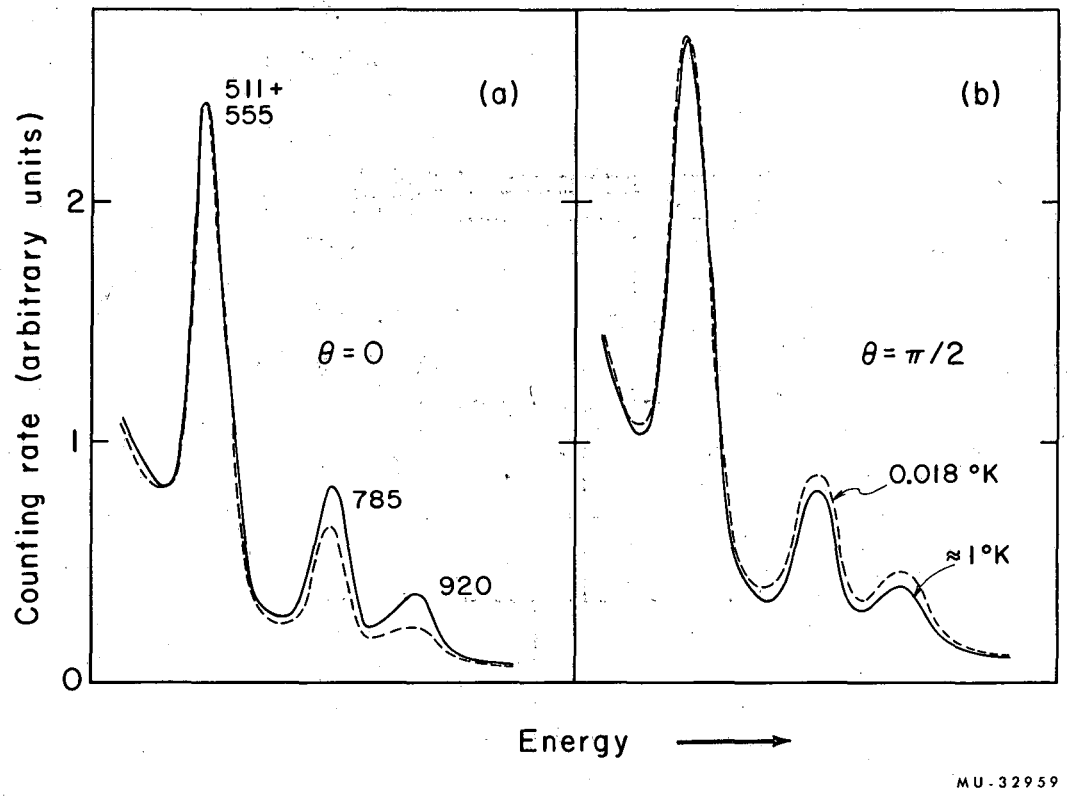

Fig. 34. Gamma-ray spectrum of Ag^{104} polarized in iron. Spectra obtained parallel and perpendicular to axis of polarization are shown. Solid curves are isotropic spectra normalized to cold counting period. Dashed curves are for $1/T \approx 60$.

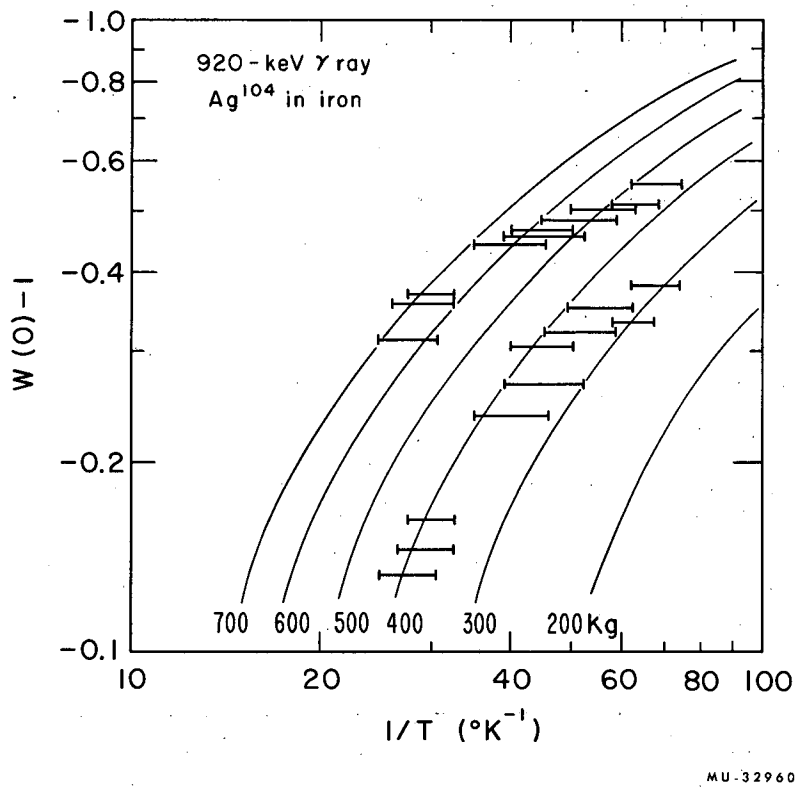

Fig. 35. W(0)-1 for 920-keV γ ray from Ag^{104} as function of temperature. Two extreme values are shown at each temperature. Curves are for various values of the hyperfine field.

anisotropy are shown. These correspond to two extreme methods of evaluating the correction for background radiation under the γ-ray photopeak. The lower set was obtained by making no background correction at all, while the upper set was obtained by making a maximum probable correction. The nature of the correction requires that the magnitude of the true anisotropy lie somewhere between these extremes. While the lower set of data is probably more nearly correct, more quantitative evaluation was impossible owing to the small intensity of the γ ray and the anisotropy of the background. The temperature range shown in Fig. 35 is that obtained by including all of the experimental variation of Fig. 10. It should be noted that the data presented in Fig. 35 were taken randomly at widely varying times and not in order of decreasing temperature. The smooth temperature variation obtained indicates that no systematic error in the temperature determination occurred such as might result from a thermal gradient from radioactive heating that decreased monotonically with time by a factor of 10 during the experiment. Such a gradient along the thermal link would have made the apparent temperature scatter quite badly.

The spins and magnetic moments of both isomers of Ag^{104} have been measured.[43,44] The values reported are μ(27-min) = + 3.7±0.2 nm and μ(69-min) = + 4.0(+0.2/-0.1)nm. The hyperfine field for silver in iron could therefore be determined, and was found to be in the range $(4.5\pm1.5)\times10^5$ G. This was actually the result for Ag^{104} in an alloy which was 5% palladium and 95% iron. Whether the palladium content alters the field from that in pure iron is not known, but the variation is probably minor compared with the experimental error in the above field determination.

The 920-keV γ ray was used for this determination because the U_2, U_4, F_2, and F_4 for it may be calculated exactly, if the spin of the 1340-keV level is taken to be 2+. The large negative values of W(0)-1 observed for this γ ray indicated that this spin assignment is correct.

The temperature dependence of $W(\theta)$ for the 785-keV γ ray is shown in Fig. 36. The temperatures here are the same as shown in

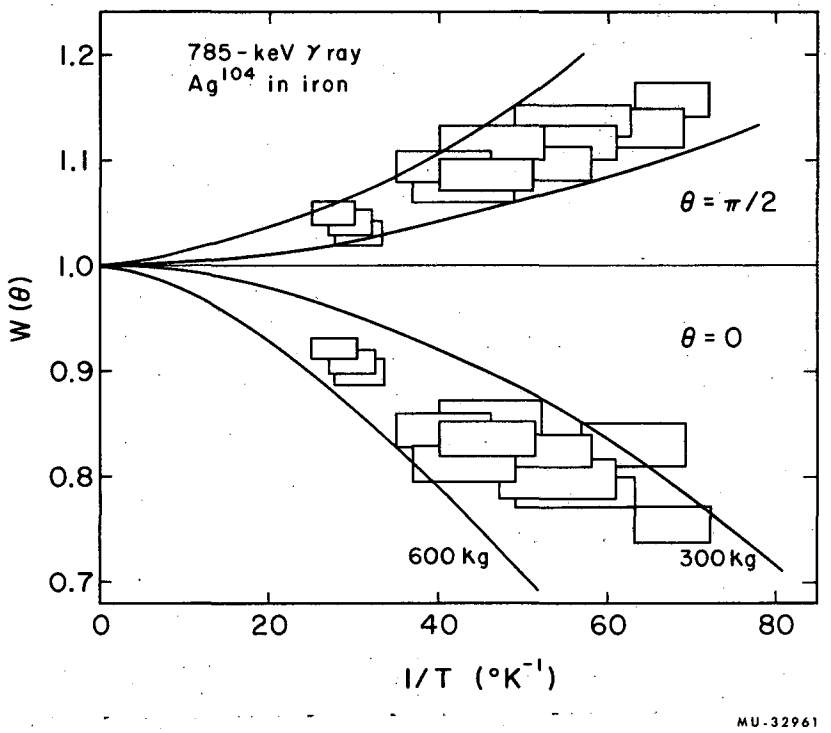

Fig. 36. $W(\theta)$ as function of $1/T$ for 785-keV γ ray from Ag^{104} polarized in iron. Curves shown are for 300 kG and 600 kG and the $F_2(785)$ value used in text.

Fig. 35. The extreme values of $W(\theta)$ are more nearly the same for this γ ray than for the 920-keV γ ray because the intensity of this transition is larger and the background is correspondingly less important. The value of $W(\theta)$ does not allow an independent determination of the hyperfine field because the M1-E2 mixing ratio for this γ ray is not known. The field value obtained above can be used to determine an approximate value for δ, however. First the value of U_2 was calculated. Then for B_2 between 0.15 and 0.44 for 300 kG and 600 kG, respectively, F_2 was found to be $F_2(785) = -1.0 \pm 0.5$. This allowed $0 \leq \delta \leq +4$ with from 0 to 80% E2 character.

The sign of the hyperfine field was determined by observing the asymmetry of the positron decay when the alloy was cooled and polarized. The sign determination is unambiguous in this case because the sign of the magnetic moment is known to be positive and the positron transition is 5+ to 4+. This latter fact requires $A_+ = +1/6$ for this pure Gamow-Teller transition. With these signs for the parameters in Eq. (9) the asymmetry may be used to yield the sign of the hyperfine field.

The counting rate of high-energy positrons in a narrow energy range is shown in Fig. 37. This figure represents two demagnetizations with the magnetizing field direction reversed. For $\theta = 0$, the polarized counting rate is clearly less than the extrapolated isotropic counting rate. Therefore, the result was $W(0) < 1$, which requires that the field at the nuclei of silver dissolved in iron be negative. This was confirmed by observing that $W(\pi) > 1$, as shown in the lower part of Fig. 37.

Identification of the source of the positrons was less clear. Several facts support the premise that only the 69-min isomer remained in appreciable intensity when the experiments shown in Fig. 37 were performed. Even though this isomer is reported to decay primarily by electron capture, appreciable positron branching exists. Evidence for this was also shown by the isotropy of the 555-keV region of the γ-ray spectra. First, the positron counting periods were recorded over 5 hr after the end of bombardment. This allowed over 10 half-lives for

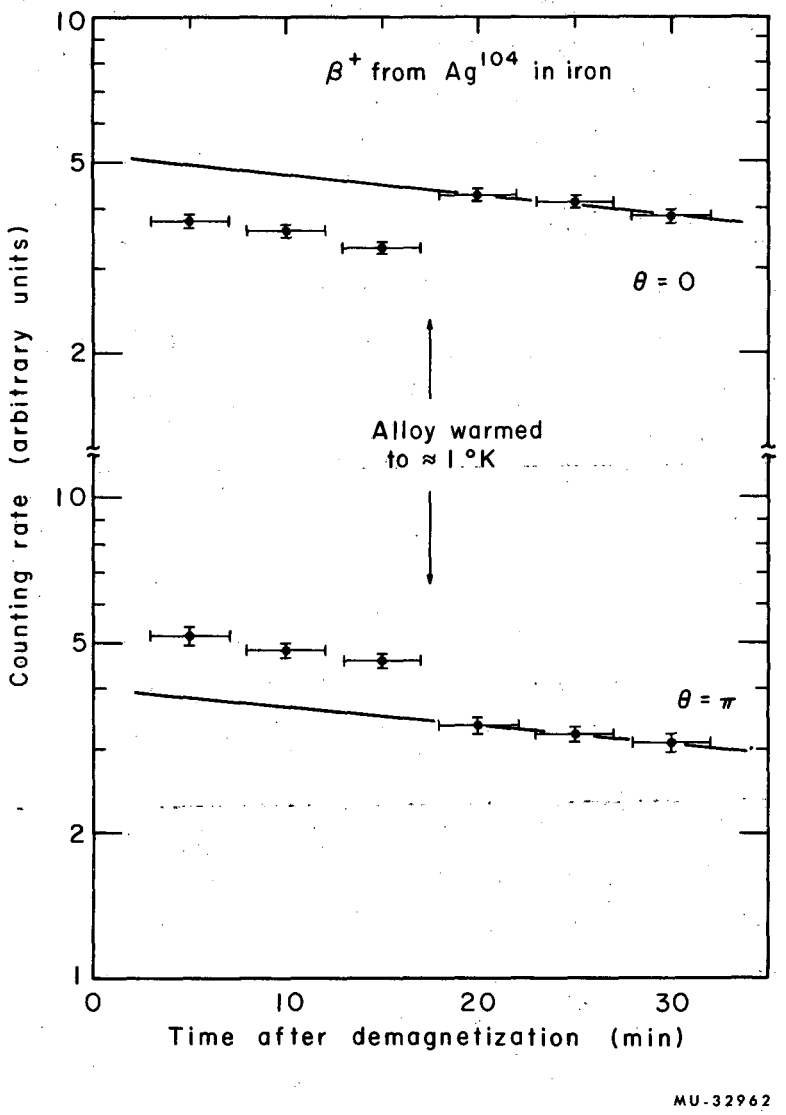

Fig. 37. Positron counting rate as function of time after demagnetization. Note that $W(0) < 1$ and $W(\pi) > 1$ for positrons indicating a negative hyperfine field.

decay of the 27-min activity. If the initial production ratio of the two isomers was roughly unity, the 27-min activity would have decreased by more than 10^3 in this time. Second, the isotropic counting rate of the 785-keV and 920-keV γ rays taken at the same time as the positron data showed essentially equal, approximately 70-min decay rates. The 785-keV γ ray thus showed no feeding by a high-energy positron branch from the 27-minute isomer. Furthermore, the positron decay rate itself showed roughly a 70-min half-life on the average, although this varied somewhat and increased slightly in time. This may be due to some effect in the germanium counter itself. Also, the γ-ray peaks and the positron counting rate disappeared into the background at about the same time. The end-point energy of the positron spectrum was estimated by a comparison of the required amplifier gain to the gain required for the 530-keV electron end point of Ag^{110m}. The positron end point was definitely not more than 1.5 MeV. The lowest intense branch from the 27-min isomer is 1.9 MeV, while the highest branch from the 69-min state is about 1.2 MeV. For these reasons the positron asymmetry has been interpreted by using the 69-min I = 5 level as their source.

The magnitude of the hyperfine field for Ag^{104} in iron obtained above, and the previously derived magnitude of μH for Ag^{110m}, allowed the magnetic moment of Ag^{110m} to be estimated. In the same way, the sign of the magnetic moment was determined exactly. The value obtained was $\mu(Ag^{110m}) = +2.0 \pm 0.6$ nm. The sign and magnitude of the hyperfine field for Ag^{110m} in nickel may also be estimated by using this value for the moment. The field in nickel was found to be $-(1.5 \pm 0.5) \times 10^5$ G.

The experimental value for the moment of Ag^{110m} is only somewhat larger than the value which may be calculated by using the shell model states $g_{9/2}$ for the 47th proton and $g_{7/7}$ for the 63rd neutron. A simple calculation of the g factors for these particles coupled to I = 6 gave $\mu(Ag^{110m}) = +1.55$ nm.

VII. DISCUSSION

A. Other Methods

Several other experimental methods have been devised for measurement of the internal fields in metals. Two of these apply spectroscopic techniques and are considerably more accurate than the other two methods, which entail averaging processes.

Nuclear magnetic resonance in ferromagnetic metals is both a precise and an accurate method.[45] Internal fields may be measured to within a few hundred gauss (< 0.1%), which is an order of magnitude better than the accuracy of any of the other methods. The sign of the field may also be determined by this method. An advantage of NMR is that the temperature dependence of the internal field may be studied over a wide temperature range.

In NMR the resonant nuclei are those in the domain walls, since only these may undergo the required transition. This fact has produced some doubt about the validity of using the measured fields as characteristic of the properties within the domains. Comparison of the NMR measurement[46] for Fe^{57} in iron with that of the other spectroscopic method[47] shows good agreement, however.

Special application of the Mössbauer effect allows both the sign and magnitude of the internal field to be measured.[12] This spectroscopic method has a accuracy of about 10% for this type of measurement. Like NMR, this method can detect the existence of more than one magnetic site and measure each of the fields independently. The field at nuclei within the domains is measured by observation of the recoil-free resonate absorption of γ radiation. Knowledge of several intrinsic nuclear parameters is thus required. Application of this method is limited by the fact that only certain isotopes exhibit recoil-free resonance absorption.

The oldest, but least accurate method, consists of measurement of the nuclear part of the heat capacity of the metal alloy.[48] The reliability of this method is reduced by effects of structure and internal strain. The sign of the field cannot be determined and only an average

field is obtained. Quite concentrated alloys are required and thus problems of miscibility and possible additional interactions are introduced.

By comparison, the method of low-temperature nuclear polarization is less accurate than the two spectroscopic methods but can be made more accurate than heat-capacity measurements for determination of internal fields. The accuracy can be better than 10% and is limited by the accuracy with which the B_k functions may be determined. Considerable knowledge about the decay scheme of the isotope used must exist or be obtainable from the experiments, however. Again, only an average field is obtained. An advantage here is that extremely dilute alloys may be used.

B. Comparison with Other Work

The decay scheme of Ag^{110m} has been the subject of several recent papers.[36, 37, 49] The polarization data were found to be consistent with the best decay scheme available and lend support to its acceptibility. No datum was obtained to indicate that a revision of the partial decay scheme was necessary.

A detailed comparison of the polarization data and the best angular-correlation measurements has already been made in Sec. VI-A. The two methods are shown to yield essentially identical results. The polarization data allow somewhat narrower limits of error to be set for the F_2 coefficients of several γ rays and the E2/M1 mixing ratios of two γ rays in Cd^{110}. The spins of the 2161-keV, 2218-keV, and 2925-keV levels in Cd^{110} were determined to be 3+, 4+, and 5+, respectively.

The internal magnetic field at silver nuclei in iron and nickel cannot be compared to other work directly as no other measurements are available. An interesting internal comparison my be made, however. The ratio of the μH product for Ag^{110m} in nickel to that for Ag^{110m} in iron is 0.39±0.04. Thus the ratio of the internal field at silver in nickel and iron is also 0.39±0.04. This ratio would be essentially the same for any silver isotope, since the field is electronic in

origin and depends upon the interaction of the silver-electronic configuration with that of the ferromagnetic atoms.

The internal fields for several other elements dissolved in iron and nickel have been determined. For Mn, the above ratio of fields is 1.9,[50, 51] for Fe it is found to be 0.77,[45, 52] and for Co it is 0.41.[33, 35] Perhaps of more importance for comparison is the ratio of the fields for diamagnetic impurities and especially the other two IB group elements. The ratio of the internal fields for Cu is 0.21,[10, 11] while for Au it is 0.23.[12] The ratios for copper and gold are seen to be closely the same, while that for silver is nearly double these values. There is some evidence that these ratios have a meaningful interpretation and that they might be expected to be roughly the same for elements with similar electronic configurations. An explanation for the larger ratio obtained with the silver alloys would be interesting.

Many factors contribute to the magnetic field at the nucleus and these are discussed in the next section. It should be noted now, however, that the large size of the impurity atoms, which cause local distortion of the ferromagnetic lattice and hence change the overlap of the electron wave functions, must play a significant role in the magnitude of the field. Of the elements copper, silver, and gold, silver has the largest atomic radius, while the radius of nickel is just slightly less than that of iron (1%). The radius of silver is 14% larger than iron. These factors alone, however, cannot explain the large ratio of the fields found for silver, since about the same distortion would be expected in the two hosts.

In Fig. 38 the experimental internal magnetic field for copper and gold is plotted against the effective atomic moment of the ferromagnetic host. The strong linear correlation between these quantities for these elements leads to the assumption that the silver fields should lie somewhere intermediate between the copper and gold lines. The field values obtain from polarization of Ag^{104} are also shown in Fig. 38. The intermediate position of the silver-alloy field points is evident.

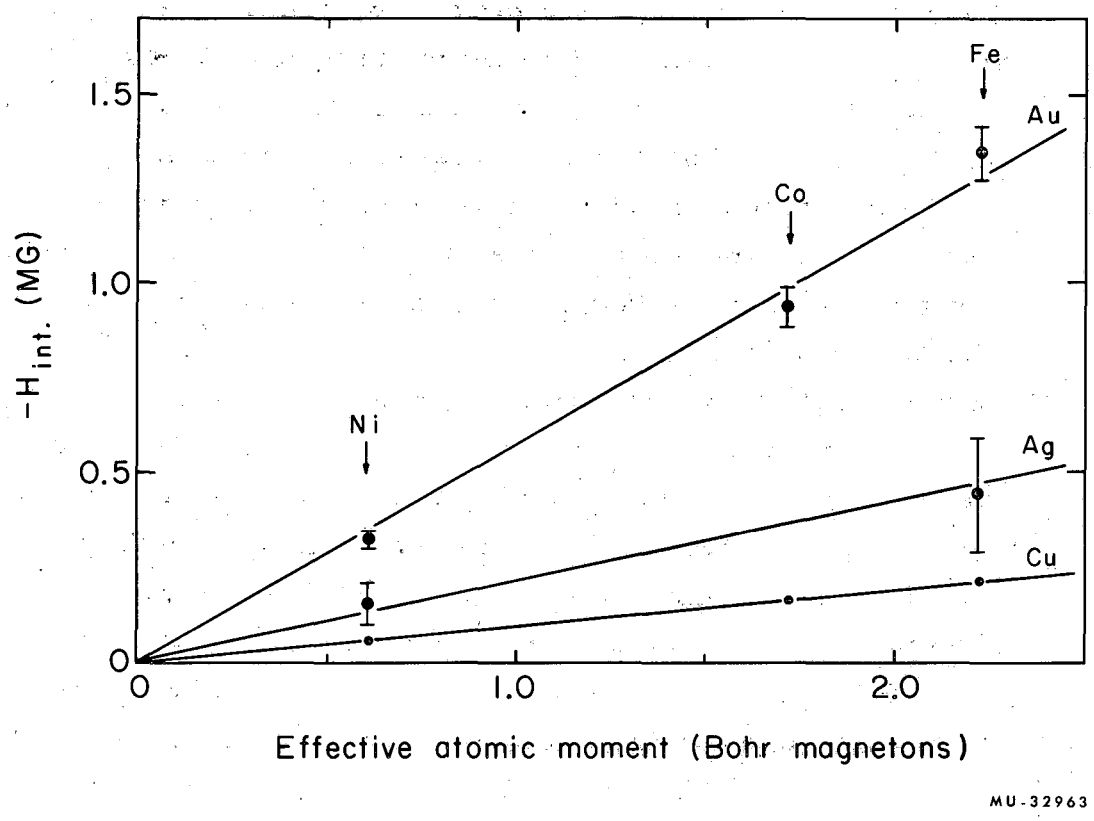

Fig. 38. Internal fields for copper, silver, and gold plotted against the effective atomic moment of the host. The silver points are for Ag^{104}.

C. Origin of the Internal Field

The first treatment of the origin of the internal magnetic field in ferromagnetic metals was performed for the cobalt nuclei in cobalt metal.[53] In this work the dominance of the negative contributions to the field was not correctly recognized. A more recent estimate[9] included the experimental fact that a large negative contribution exists.[5]

Several mechanisms have been advanced that give rise to negative contributions to the hyperfine field of ferromagnetic atoms. Of present concern, however, is the hyperfine field of nonmagnetic atoms dissolved in ferromagnetic hosts. The nonmagnetic atoms cannot of themselves be the origin of the observed field, since the free atoms have no net unpaired spin. Some alteration of the electronic wave functions about the nuclei of a nonmagnetic atom must thus occur when the atom is dissolved in the ferromagnet. Only the outer electrons have appreciable overlap, so the interaction probably occurs by a mechanism in which these electrons play a prominent role. Such a mechanism is the conduction-electron polarization mechanism to be described below.

Calculations have shown that the electron-spin density in the outer regions of transition-metal atoms is directed antiparallel to the unpaired 3d spin direction.[54, 55] In the metal, the 3d electrons are locked parallel by ferromagnetic exchange. The 4s wave functions of these atoms are the only ones which have large amplitudes outside the maxima of the 3d functions. Thus the 4s electrons have a net spin density which is opposed to the inner 3d spins.

A simple qualitative way of constructing this effect is to suppose that 4s electrons with opposite spin may have different radial wave functions. Then, a 4s electron with spin parallel to the 3d spins will feel exchange forces and be drawn in toward the maximum 3d spin density leaving those with opposite spin on the outside of the atom.

Parenthetically, it should be pointed out that since the electronic g factor is negative, the 3d spin (the orbital part is presumed to be quenched) produces a negative contribution to the hyperfine field through its dipolar effect. Since the 4s electrons with spin parallel to the 3d

spins are normalized to a smaller volume, the net 4s spin density at the nucleus is also parallel to the 3d spins. The 4s contribution to the field via the Fermi contact interaction is, however, positive, but small by comparison with the 3d contribution. The dominance of the negative contribution is of course found to be the case experimentally.

The 4s electrons thus contribute a polarized spin density to the conduction band of the metal. These "conduction" electrons are free in the sense that they may interact easily with neighboring atoms but are yet relatively localized, having a periodicity characteristic of the lattice.

The outer electrons of the nonmagnetic solute atoms are thus bathed in a sea of electrons which have a net spin density opposed to the 3d spins of the ferromagnetic atoms. Exchange between these electrons then gives rise to the magnetic effects observed in the nonmagnetic atoms. The assumption of a positive exchange integral[54] for the outer 4s electrons of the ferromagnetic atoms and the outer s electrons (5s in the case of silver) of the nonmagnetic atoms leads directly to a large negative contribution to the field at the nucleus of the nonmagnetic atoms.

The magnitude of the field will thus depend upon the magnitude of the unpaired spin density in the outer regions of the ferromagnetic atoms and upon the extent of overlap between the wave functions. Since the magnitude of the unpaired 4s spin density depends directly on the 3d spins, the field in the nonmagnetic atoms should show a correlation with the effective magnetic moments of the 3d spins. This correlation has already been shown in Fig. 38 for the nonmagnetic IB group elements dissolved in iron, cobalt, and nickel. The relationship is apparently linear in the 3d spin. A conduction-electron polarization mechanism is, thus, entirely consistent, in a qualitative way, with the observed magnetic effects.

It would be desirable, of course, to be able to predict the magnitude as well as the sign of the hyperfine field for any element dissolved in a ferromagnetic host. Since rigorous calculations are not

yet possible, a semi-empirical approach must be used. The hyperfine field created upon dissolving a diamagnetic element in a ferromagnetic metal is produced by perturbation of the electrons of the diamagnetic atom itself. Because the orbital momentum of non-s electrons is quenched, only the s electrons have a large effect on the nucleus via the contact interaction. The s electrons are therefore of particular importance in metals. An investigation of the s electron contribution to the ordinary hyperfine structure of free atoms and ions may lead to a relationship that is useful for metals.

Optical spectra of the elements and monovalent ions give values for the s-electron contribution to the hyperfine-structure constant, a_s. This parameter allows calculation of both the s-electron density at the nucleus and the resulting effective hyperfine field.[56] The field is found to vary with atomic number in a relatively smooth manner. The derived fields are plotted against atomic number in Fig. 39.

In metals the weak overlap of the polarized conduction electrons with the electrons of the nonmagnetic atom causes a reduction in the magnitude of the field observed in the metals from that of the free atom or ion. If the overlap of the outer conduction electrons is assumed to be about the same for all atoms, the curves of Fig. 39 may be scaled down appropriately and compared with the fields found in metals. In Fig. 40 the curves of Fig. 39 have been scaled linearly and fitted to the best experimental value for Au in iron. The other points shown are all experimental field values observed when the element is dissolved in iron. The correlation, although poor, is unmistakable. Even a 30% accuracy in the predictions of this rudimentary theory, which uses but one mechanism and which contains many assumptions, is rather gratifying.

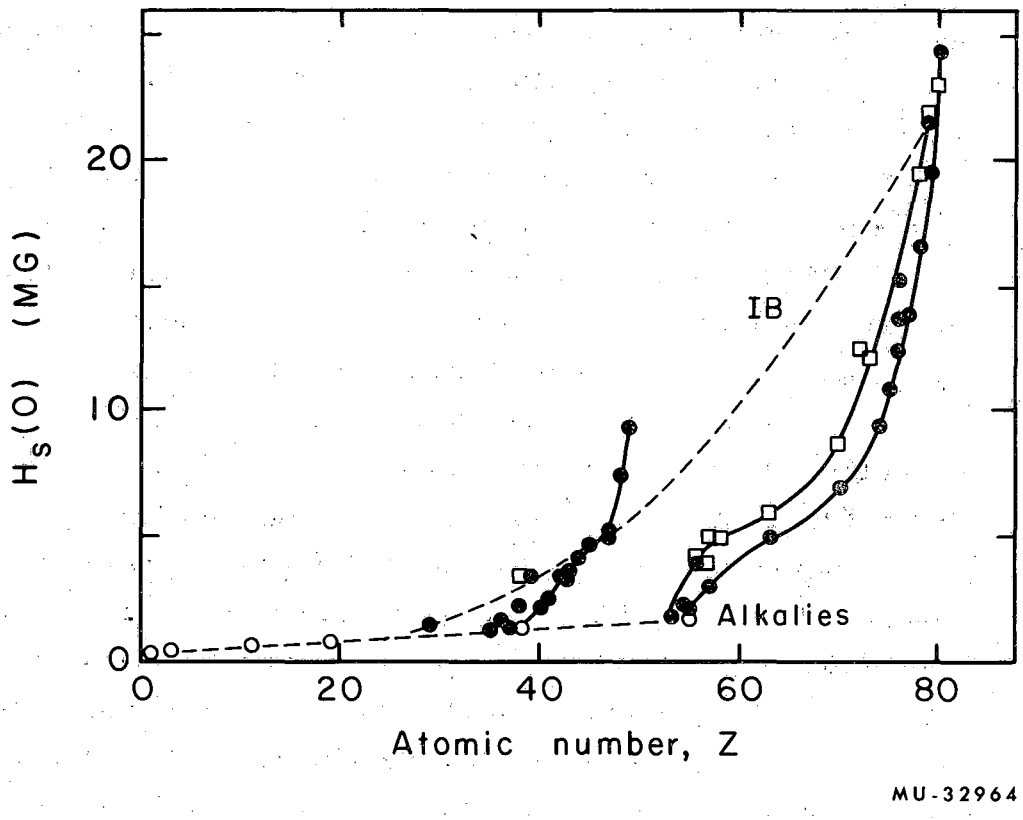

Fig. 39. Plot of s electron contribution to hyperfine field as function of atomic number.

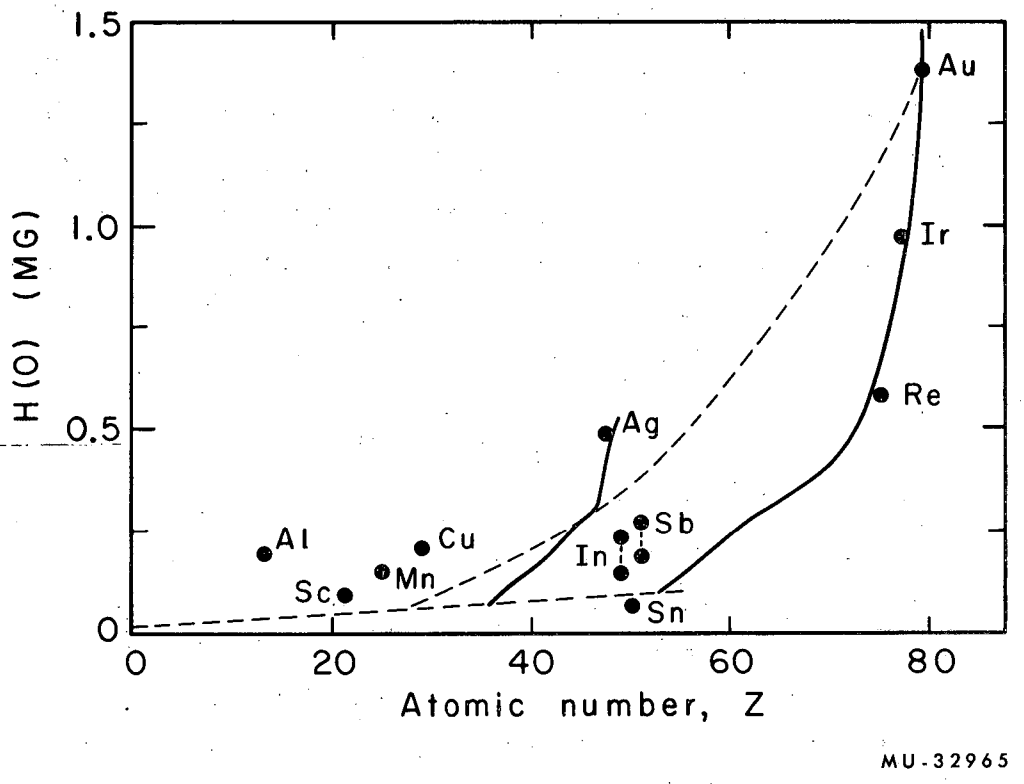

Fig. 40. Experimental hyperfine fields in iron plotted against atomic number. Curves are from Fig. 39 fitted to the experimental value of Au in iron.

D. Conclusions

Knowledge of the decay of Ag^{110m} has been extended by establishment of the multipole character of four γ rays in Cd^{110} as pure E2 transitions. Two transitions of mixed multipolarity have been characterized, with the result that the 1383-keV γ ray is 11±1% E2 and the 1504-keV γ ray is <1% E2.

The internal magnetic field at cobalt in nickel was established independently and was found to be in excellent agreement with a recent NMR measurement. The best value obtained was 120 kG.

The signs and magnitudes of the hyperfine interactions of Ag^{110m} in iron and nickel were obtained. The sign of the product μH was determined to be negative for both alloys. For Ag^{110m} in iron this was found to be $\mu H = -(9.0 \pm 0.5) \times 10^5$ nm gauss and for Ag^{110m} in nickel $\mu H = -(3.0 \pm 0.3) \times 10^5$ nm gauss.

The 69-minute isomer of Ag^{104} was also polarized and the internal field in a 5% Pd in iron alloy was found to be negative. The magnitude of the field in this alloy was determined to be $-(4.5 \pm 1.5) \times 10^5$ G, which allowed determination of the sign and estimation of the magnitude of the magnetic moment of Ag^{110m}. The moment is +2.0±0.6 nm, which agrees with a naive calculation. If the moment of Ag^{110m} given above is accepted, the internal field at silver nuclei in nickel is $-(1.5 \pm 0.5) \times 10^5$ G.

The internal field at silver nuclei dissolved in iron and nickel was shown to be approximately predicted by a rudimentary theory.

ACKNOWLEDGMENTS

It is my privilege to acknowledge the contributions of many others to this work; I especially thank:

Professor David A. Shirley, who directed this research, for his help in overcoming many experimental problems and for explanation of many concepts.

My wife, Elizabeth, for her unfailing patience and kind encouragement.

Mr. G. G. Young, Mr. D. N. Voronin, and Mr. M. K. Flamm for unexcelled mechanical performance in the construction of the vacuum and other equipment.

Mr. Harry S. Powell and his staff for fabrication of the glass Dewars and early cryostat assemblies.

Mr. Richard B. Frankel, a fellow student, for an unending supply of reliable low-temperature beta counters and for advice and help in their use.

Dr. John G. Conway for the use of his high-temperature furnace.

Mr. Clinton N. Ward for his help with electronic problems of every type.

Dr. Ronald W. Grant for many scientific and unscientific discussions.

And my fellow students: Mr. H. Hollis Wickman, Mr. Richard M. Levy, Mr. Richard B. Frankel, and Mr. Johan Blok for many interesting hours--both profitable and otherwise.

REFERENCES

1. B. N. Samoilov, V. V. Sklyarevskii, and E. P. Stepanov, Zh. Eksptl. i Teoret. Fiz (USSR) 36, 644 (1959); Soviet Phys. JETP (English Transl.) 9, 448 (1959).
2. B. N. Samoilov, V. V. Sklyarevskii, and E. P. Stepanov, Zh. Eksptl. i Teoret. Fiz. (USSR) 36, 1944 (1959); Soviet Phys. JETP (English Transl.) 9, 1383 (1959).
3. B. N. Samoilov, V. V. Sklyarevskii, and E. P. Stepanov, Zh. Eksptl. i Teoret. Fiz. (USSR) 38, 359 (1960); Soviet Phys. JETP (English Transl.) 11, 261 (1960).
4. A. J. F. Boyle, D. St. P. Bunbury, and C. Edwards, Phys. Rev. Letters 5, 553 (1960).
5. S. S. Hanna, J. Heberle, G. J. Perlow, R. S. Preston, and D. H. Vincent, Phys. Rev. Letters 4, 513 (1960).
6. B. N. Samoilov, V. V. Sklyarevskii, and V. D. Gorobchenko, Zh. Eksptl. i Teoret. Fiz. (USSR) 41, 1783 (1961); Soviet Phys. JETP (English Transl.) 14, 1267 (1962).
7. C. Roberts and J. M. Winter, Compt. Rend. 250, 3831 (1960).
8. R. E. Watson and A. J. Freeman, Phys. Rev. 123, 2027 (1961).
9. D. A. Goodings and V. Heine, Phys. Rev. Letters 5, 370 (1960).
10. T. Kushida, A. H. Silver, Y. Koi, and A. Tsujimura, J. Appl. Phys. Suppl. 33, 1079 (1962).
11. K. Asayama, S. Kobayashi, and J. Itoh, J. Phys. Soc. Japan 18, 458 (1963).
12. R. W. Grant, Study of the Nuclear Zeeman Effect in Au^{197} (Ph. D. Thesis), Lawrence Radiation Laboratory Report UCRL-10649, January 1963 (unpublished).
13. J. W. T. Dabbs, L. D. Roberts, and S. Bernstein, Phys. Rev. 98, 1512 (1955).
14. R. J. Blin-Stoyle and M. A. Grace, Oriented Nuclei, in Handbuch der Physik, ed. by S. Flugge (Springer-Verlag, Berlin, 1957) p. 556.

15. M. J. Steenland and H. A. Tolhoek, Orientation of Atomic Nuclei at Low Temperatures, in Progress in Low Temperature Physics II, ed. by C. J. Gorter (North-Holland Publishing Company, Amsterdam, 1957), p. 292.

16. H. A. Tolhoek and J. A. M. Cox, Physica 19, 101 (1953).

17. T. D. Lee and C. N. Yang, Phys. Rev. 104, 254 (1956).

18. C. S. Wu, E. Ambler, R. W. Hayward, D. D. Hoppes, and R. P. Hudson, Phys. Rev. 105, 1413 (1957).

19. W. J. Huiskamp and H. A. Tolhoek, Orientation of Atomic Nuclei at Low Temperatures III, in Progress in Low Temperature Physics III, ed. by C. J. Gorter (North-Holland Publishing Company, Amsterdam, 1961) p. 333.

20. H. Postma, W. J. Huiskamp, A. R. Miedema, M. J. Steenland, H. A. Tolhoek, and C. J. Gorter, Physica 23, 259 (1957).

21. E. Ambler, R. W. Hayward, D. D. Hoppes, and R. P. Hudson, Physica 24, 64 (1958); and Phys. Rev. 110, 787 (1958).

22. E. Ambler, R. W. Hayward, D. D. Hoppes, and R. P. Hudson, Phys. Rev. 106, 1361 (1957); and 108, 503 (1957).

23. R. A. Erickson, L. D. Roberts, and J. W. T. Dabbs, Rev. Sci. Instr. 25, 1178 (1954).

24. Q. O. Navarro, Preferential Polar Alpha-Particle Emission in Oriented Californium and Einsteinium (Ph. D. Thesis), Lawrence Radiation Laboratory Report UCRL-10362, July 1962 (unpublished).

25. R. B. Frankel (Lawrence Radiation Laboratory), private communication.

26. A. J. Dornblatt, Trans. Electrochem. Soc. 74, 280 (1938).

27. M. Hansen, Constitution of Binary Alloys (McGraw-Hill Book Company, Inc., New York, 1958), p. 36.

28. M. A. Grace, C. E. Johnson, N. Kurti, R. G. Scurlock, and R. T. Taylor, Phil. Mag. 4, 948 (1959).

29. A. C. Anderson, G. L. Salinger, and J. C. Wheatley, Rev. Sci. Instr. 32, 1110 (1961).

30. J. C. Wheatley, D. F. Griffing, and T. L. Estle, Rev. Sci. Instr. 27, 1070 (1956).

31. J. A. Beun, A. R. Miedema, and M. J. Steenland, Physica 23, 1 (1957).

32. J. M. Daniels and N. Kurti, Proc. Roy. Soc. (London) A221, 243 (1954).

33. Y. Koi, A. Tsujimura, T. Hihara, T. Kushida, J. Phys. Soc. Japan 16, 1040 (1961).

34. V. Arp, D. Edmonds, and R. Petersen, Phys. Rev. Letters 3, 212 (1959).

35. R. C. LaForce, S. F. Ravitz, and G. F. Day, Proc. Int. Conf. Magnetism Crystallography, Kyoto, Japan, 1961, J. Phys. Soc. Japan 17, Suppl. B-1, Mar. 1962, p. 99.

36. T. Katoh and Y. Yoshizawa, Nucl. Phys. 32, 5 (1962).

37. E. G. Funk, Jr. and M. L. Wiedenbeck, Phys. Rev. 112, 1247 (1958).

38. G. A. Westenbarger and D. A. Shirley, Phys. Rev. 123, 1812 (1961).

39. M. Ferentz and N. Rosenzweig, Table of F Coefficients, Argonne National Laboratory Report ANL-5324, 1955.

40. Nuclear Data Sheets, NRC 60-2-62 (1960) (National Academy of Sciences, National Research Council).

41. H. Daniel, O. Mehling, and D. Schotte, Z. Physik 172, 202 (1963).

42. R. K. Girgis and R. van Lieshout, Nucl. Phys. 13, 493 (1959).

43. O. Ames, A. M. Bernstein, M. H. Brennan, and D. R. Hamilton, Phys. Rev. 123, 1793 (1961).

44. O. Ames, A. M. Bernstein, M. H. Brennan, R. A. Haberstroh, and D. R. Hamilton, Phys. Rev. 118, 1599 (1960).

45. A. C. Gossard and A. M. Portis, Phys. Rev. Letters 3, 164 (1959).

46. J. I. Budnick, L. J. Bruner, R. J. Blume, and E. L. Boyd, J. Appl. Phys. 32, 1205 (1961).

47. S. S. Hanna, J. Heberle, C. Littlejohn, G. J. Perlow, R. S. Preston, and D. H. Vincent, Phys. Rev. Letters 4, 177 (1960).

48. C. V. Heer and R. A. Erickson, Phys. Rev. 108, 896 (1957).
49. H. W. Taylor and S. A. Scott, Phys. Rev. 114, 121 (1959).
50. J. A. Cameron, R. A. G. Lines, B. G. Turrell, and P. J. Wilson, Phys. Rev. Letters 4, 323 (1963).
51. Y. Koi and A. Tsujimura, J. Phys. Soc. Japan 18, 1347 (1963).
52. G. K. Wertheim, Phys. Rev. Letters 4, 403 (1960).
53. W. Marshall, Phys. Rev. 110, 1280 (1958).
54. A. J. Watson and R. E. Freeman, Phys. Rev. Letters 6, 277 (1961).
55. A. J. Freeman and R. E. Watson, Phys. Rev. Letters 5, 498 (1960).
56. H. Kopfermann, Nuclear Moments (Academic Press, Inc., New York, 1958).

This report was prepared as an account of Government sponsored work. Neither the United States, nor the Commission, nor any person acting on behalf of the Commission:

A. Makes any warranty or representation, expressed or implied, with respect to the accuracy, completeness, or usefulness of the information contained in this report, or that the use of any information, apparatus, method, or process disclosed in this report may not infringe privately owned rights; or

B. Assumes any liabilities with respect to the use of, or for damages resulting from the use of any information, apparatus, method, or process disclosed in this report.

As used in the above, "person acting on behalf of the Commission" includes any employee or contractor of the Commission, or employee of such contractor, to the extent that such employee or contractor of the Commission, or employee of such contractor prepares, disseminates, or provides access to, any information pursuant to his employment or contract with the Commission, or his employment with such contractor.